International Atomic Energy Agency

INDC(CCP)-403
Distr.: L

INDC INTERNATIONAL NUCLEAR DATA COMMITTEE

SELECTED ARTICLES TRANSLATED FROM JADERNYE KONSTANTY (NUCLEAR CONSTANTS) VOLUMES 3 - 4, 1994

Translated by the IAEA

June 1997

IAEA NUCLEAR DATA SECTION, WAGRAMERSTRASSE 5, A-1400 VIENNA

Reproduced by the IAEA in Austria
June 1997

INDC(CCP)-403
Distr.: L

SELECTED ARTICLES TRANSLATED FROM JADERNYE KONSTANTY (NUCLEAR CONSTANTS) VOLUMES 3 - 4, 1994

Translated by the IAEA

June 1997

CONTENTS

95-11660 (H)
Translated from Russian

NEUTRON CONSTANTS AND PARAMETERS

News from the Nuclear Data Centre

Publications of recent years have carried the results of new measurements of a number of quantities which differ considerably from those published and accepted previously. In this connection the Nuclear Data Centre considers it necessary to provide information on the following significant changes in nuclear data that are important for practical applications:

1. The previously accepted half-life for the radionuclide $^{108}Ag^{m}$ was 127 ± 7 years. In Ref. [1], reporting on work performed in Brunswick, a value of 418 ± 15 years was obtained;
2. The capture cross-section for ^{90}Sr at the thermal point included in the BNL Atlas [2] was 0.9 ± 0.5 b. The latest measurements [3] show a value of 9.7 ± 0.7 mb.

[1] SCHOETZIG, U. et al., Precision measurements of radioactive decay data, Proc. Int. Conf. on Nucl. Data for Sci. and Techn., Juelich (1991) 562.

[2] Neutron Cross Sections, Vol. 1, Neutron resonance parameters and thermal cross-sections. Part A, New York (1981).

[3] LONE, M.A. et al., Measurement of the thermal neutron cross-section of the $^{90}Sr(n,\gamma)^{91}Sr$ reaction, Nucl. Instr. and Methods in Phys. Research (1993).

V.N. Manokhin
Director of the Nuclear Data Centre

UDC 539.172

TESTING NEUTRON CROSS-SECTION FILES FROM THE BROND-2 AND ENDF/B-6 LIBRARIES IN BENCHMARK EXPERIMENTS ON NEUTRON TRANSMISSION THROUGH SPHERICAL LAYERS

A.A. Androsenko, P.A. Androsenko, A.I. Blokhin, N.T. Kulagin, V.G. Pronyaev and S.P. Simakov

Institute of Physics and Power Engineering, Obninsk

ABSTRACT

The effect of angular anisotropy in inelastic secondary neutron scattering on neutron leakage spectra from the surface of spherical specimens is investigated. It is shown how inadequate representation of the cross-section structure in the neutron energy resonance region can affect the neutron leakage spectrum.

The international thermonuclear experimental reactor project ITER is entering a new phase - the engineering design phase. An evaluated nuclear data library FENDL [1] is being set up to facilitate the supplying by the international scientific community of the necessary constants for the nuclear physics part of the engineering calculations, this being co-ordinated by the IAEA. The library comprises files of evaluated neutron cross-sections from the national libraries ENDF/B-VI (USA), JENDL-3 (Japan), EFF-2 (Western Europe) and BROND-2 (CIS).

The requirements for nuclear data and also their contemporary status are discussed in the survey in Ref. [2]. The reports in Ref. [3], presented at the IAEA Advisory Group Meeting on FENDL-2 and Associated Benchmark Calculations, show that benchmark experiments for complex multi-component or extended systems are often reproduced unsatisfactorily in calculations. As a rule, this is explained by gross errors in the macroscopic group cross-sections, whose cause is to be found either in the methods of

presenting the original files of evaluated microscopic nuclear cross-sections or in the procedure for preparing the group cross-sections from these files.

At the same time another possible cause of the notable discrepancies may be the generally unsatisfactory quality of the microscopic data. A clear answer to the question of the quality of the microscopic evaluated data for different materials can be given only by analysing benchmark experiments carried out in simple geometry for single component materials. Such experiments include measurements of the partial or total leakage of neutrons and their energy spectra from a 14 MeV neutron source located at the centre of a spherical shell made of the material under investigation. A large number of benchmark experiments and calculations of this kind have served to improve the representation of secondary neutron emission spectra in the hard region and to provide indications as to the quality of description of the (n,2n) cross-sections in the evaluated data files.

The purpose of this work is to try and answer two questions concerning the representation of nuclear data in evaluated cross-section files and the calculation of neutron transport in systems with spectra characteristic of thermonuclear devices:

1. Does allowance for anisotropy in the shape of the angular distributions for the continuous part of the secondary neutron spectrum have a great effect on the neutron leakage spectra?
2. Is the fact that the experimental data considerably exceed the calculated values for the leakage spectra of secondary neutrons with energies 1-5 MeV from thick spherical shells (more than three free path lengths for 14 MeV neutrons) not due to inadequate representation of the cross-section structure in the evaluated neutron cross-section files?

Effect of allowance for anisotropy in the form of the angular distributions of the continuous part of the secondary spectrum on neutron leakage

From experimental [5] and theoretical [6] investigations of secondary neutron spectra in reactions induced by 14 MeV neutrons it is well known that the angular distributions in the hard part of emission spectra possess appreciable anisotropy with predominant leakage of neutrons at forward angles. It is evident that this circumstance may affect calculations of neutron transport in systems with geometry close to that of a thermonuclear reactor by increasing the penetration or leakage of neutrons with energies greater than 2 MeV. This also determines the higher requirements for accuracy of double differential neutron emission cross-sections (error not more than 10%) in the world list of nuclear data requirements - WRENDA [2].

However, only after switching to the evaluated neutron cross-section format in ENDF/B-6 [7] was it possible to represent the double differential cross-sections in files for the continuous spectrum region. The files of evaluated neutron cross-sections included in the FENDL library contain such data. Existing systems of programs for processing files into constants for calculating neutron transport are not sufficiently well adapted at present for operating with the ENDF/B-6 format. Therefore the question as to how much allowance for angular anisotropy in the secondary neutron emission spectra affects the description of neutron passage through media has remained open until recently. An oblique answer to this question was obtained by the authors of Ref. [8] in calculations by the discrete ordinates method of neutron leakage spectra for Be and Fe spheres with a 14 MeV source at the centre and with allowance for angular anisotropy of double differential cross-sections. The results of calculations by the Monte Carlo method in the approximation of angular isotropy of double differential cross-sections are presented in these works. As calculations have shown,

allowance for angular anisotropy has practically no effect on the magnitude of the total leakage but can appreciably affect the leakage spectrum in the neutron energy region above 2 MeV. Thus, in the case of an iron sphere 30.45 cm thick, the leakage spectrum for neutrons with energy from 2 to 12 MeV is ~ 50% higher in calculations based on files containing anisotropy in the form of angular distributions for the continuous spectrum region.

To obtain a straight answer to this question, we performed calculations of the total leakage of neutrons and their energy spectra for spherical layers of beryllium and iron for neutrons from a 14 MeV source by the Monte Carlo and discrete ordinates methods. The calculations were based on files of evaluated neutron cross-sections from the ENDF/B-6 and BROND-2 libraries containing energy-angle distributions for secondary neutrons in the continuous spectrum region in tabular form or in the form of Kalbach parametrization [12]. In the calculations account was taken of the real geometry of the sphere and the ion guide channel, the geometry of the target, absorption of neutrons by the target holder, and the energy-angle distribution of source neutrons. All the information necessary for the calculations apart from the design of the target holder is supplied in Tables 1 and 2. The effect of the target holder design on neutron yield is discussed in Ref. [9]. In comparing the experimentally-observed partial leakage spectra with the theoretical ones, the latter were not averaged over the energy with the spectrometer resolution function determined experimentally.

The results of calculations of the 4π neutron leakage spectra in comparison with experimental data are shown in Figs 1 and 2. The calculations were performed both by the Monte Carlo method with and without allowance for angular anisotropy in the continuous part of the secondary neutron spectra and by the discrete ordinates method with group description of the cross-sections and the transfer matrices. For greater clarity, Fig. 3 shows

the ratio of calculations allowing for angular anisotropy in the secondary neutron spectra to calculations in the isotropic approximation. For performing calculations by the Monte Carlo method, the BRAND [10] program was adapted so that the files of evaluated cross-sections in ENDF/B-6 format could be used directly. The calculations were performed for neutron energies above 0.2 MeV for beryllium and 1.0 MeV for iron. For calculations by the discrete ordinates method we used the ANISN program [11], the group constants for which were prepared with the aid of the NJOY-87 program. The S16P11 approximation was performed in calculations of neutron transport with allowance for angular anisotropy for all processes in the 100 group representation (GAM grouping).

The results of calculations of partial leakage with very arbitrary energy grouping of source neutrons (10-20 MeV), scattered neutrons (5-10 MeV), (n,2n) reaction neutrons (1-5 MeV) and slow neutrons (below 1 MeV) are presented in Tables 3-5 in comparison with experimental data.

After analysing these data, we come to the conclusion that allowance for angular anisotropy for the continuous part of the neutron emission spectrum:

(a) has practically no effect on the magnitude of the integral neutron leakage for spheres with a thickness several times the free path length;

(b) leads to an increase by several tens of per cent in the leakage in the "scattered" neutron group when there is a low absolute contribution by this group to the total leakage.

In view of this, the accuracy requirement for presentation of double differential cross-sections (above 10%) in the WRENDA list for thermonuclear applications is evidently exaggerated. It is possible that such a requirement needs to be maintained for the representation of energy spectra but the accuracy requirement for the representation of

angular distributions for the continuous part of the spectrum appears unjustified, and in any case it is already achieved with Kalbach and Mann's parametrization [12].

Representation of the cross-section energy structure in evaluated data files when performing benchmark calculations

The fraction of the neutron leakage spectrum with energy below a few MeV for large thicknesses of the spherical layers becomes predominant for a 14 MeV neutron source. Comparison of measurements and calculations of leakage spectra for iron spheres with a thickness of around 7 free path lengths (Δd = 30.45 cm) shows experimental values considerably - up to several times - in excess of theory [13] for the leakage spectrum in the region $1 < E_n < 5$ MeV. Such a trend was also observed for large-diameter lead spheres [14]. Attempts to attribute these discrepancies to deficiencies in the experimental data are unsatisfactory in our opinion.

Possible causes of such discrepancies may be: inadequate representation of neutron cross-section structure in evaluated nuclear data files for neutrons with energy above the resonance region, too low a value of the (n,2n) reaction cross-section and too hard a form of the secondary particle emission spectrum. For iron the upper limit of the resonance region in contemporary files is 850 keV. The cross-sections were given above in the pointwise representation with structures taken from experimental data possessing the best energy resolution. As a rule these are measurements performed on the ORELA accelerator at Oak Ridge. However as shown in Ref. [15], even data from experiments with high resolution do not enable one to describe the "observed" self-shielding factors of the total cross-section in experiments with poor resolution. The reason for this is that, even in experiments with the highest resolution for energies above the resonance region, the true structure of the cross-sections in not fully resolved. Figure 4 shows the self-shielding factors

of the total cross-sections determined in experiments with poor resolution for transmission through thick specimens in comparison with data calculated from experimental data obtained with high resolution.

To demonstrate the effect of the cross-section structure on neutron leakage, we carried out calculations of leakage spectra for an iron sphere 30.45 cm thick with different groupings and a 14 MeV neutron source. In the calculations we used the ^{nat}Fe file from the BROND-2 library, where the total cross-sections for energy above 850 keV (up to 2.1 MeV) are the total cross-sections for natural iron, measured on ORELA, while below 850 keV they are represented as the resolved resonance region. With the aid of the NJOY-87 programme, the systems of group constants were prepared in which the 19-group constant system having group boundaries above 100 keV as in the BNAB system was used as the base. It may be assumed that in the pointwise representation of the cross-sections reconstructed from the resonance parameters their structure for energies below 850 keV is on average correctly reproduced. Calculations of the total and partial neutron leakage for the energy interval 400-800 keV were performed with the aid of the ANISN programmes in the S16P3 approximation. The calculations were performed for a one-group cross-section representation in this interval for a seven-group division (GAM grouping, average group width 60 keV), for a 20-group division (20 keV) and for an 80-group division (5 keV). The group boundaries outside this energy interval were unchanged.

The results of calculations of partial neutron leakage in the energy interval 400-800 keV, based on different groupings, are shown in Table 6. The leakage spectra for 20-group and 80-group divisions are shown in Fig. 5. It should be noted that grouping with a group width less than 5 keV makes it possible to reproduce details of the cross-section structure conditioned by the contribution of the s-wave and, in particular, large dips in cross-

sections occurring with interference of resonance and potential scattering. It can be seen from the Table that partial leakage in the 400-800 keV energy interval increases by 40% with a more detailed representation of cross-sections. The total leakage in this case increases by only 1.5%, since a certain amount of compensation arises owing to its reduction in the lower groups. Evidently, in order to allow for the structure of cross-sections conditioned by the contributions of higher waves (from resonances of small width), it is necessary to have either a finer grouping or to make correct allowance in the transport calculations for self-shielding of the cross-sections.

The conclusions obtained for the 400-800 keV neutron energy interval can also be applied to higher energies (for iron and other constructional materials up to energy 3-4 MeV). This is because even with the detailed pattern of the cross-sections given in the files it is not possible to obtain the correct value of the total cross-section self-shielding coefficient (Fig. 4).

Ref. [16] presents a simple formula for improving the description of total cross-section self-shielding for the neutron energy region above resonance. This involves artificially increasing the cross-sections at the maxima and reducing them at the minima whilst maintaining the energy-averaged cross-sections. It is possible that multigroup calculations (with number of groups $\sim$ 1000 for E_n = 1-5 MeV) in the discrete ordinates method, using nuclear data files corrected by this method, will enable better agreement to be obtained with experimental results for neutron leakage spectra from thick spherical layers.

Conclusions

Consideration of the results of benchmark experiments on iron enables the following conclusions to be drawn and recommendations made for improving the file of evaluated neutron cross-sections for iron in the BROND-2 library:

1. Partial leakage in the source neutron group ($E_n > 10$ MeV) is appreciably too high, indicating too high an elastic scattering cross-section (by about 10%) at energies above 10 MeV;
2. Partial leakage in the scattered neutron group is also too high which is caused by a too hard inelastically scattered neutron spectrum with excitation of discrete low-lying levels (contribution of direct processes too high);
3. Since the total cross-section for iron given in the BROND-2 library file is known with high accuracy, while the elastic cross-section is too high, the total cross-section for inelastic processes (mainly inelastic scattering and (n,2n) reaction cross-sections), which lead to substantial softening of the leakage spectra is too low, as can be seen from the figures and tables presented here;
4. For calculating the leakage spectra in the neutron energy region below 4 MeV and up to the upper limit of the resolved resonance region, it is necessary to have detailed knowledge of the cross-section structure and to perform calculations pointwise with respect to energy or by the multigroup approach. An alternative to this could be to use small-group approaches with successive allowance for self-shielding of cross-sections.

REFERENCES

[1] Fusion Evaluated Nuclear Data Library (FENDL), Proc. IAEA Specialists Meeting on Fusion Evaluated Nuclear Data Library, IAEA, Vienna, 8-11 May 1988 (Goulo, V., Ed.) IAEA, Vienna (1989).

[2] SCHMIDT, J.J., Acta Physica Hungarica, 69, (3-4) (1991) 269.

[3] YOUSSEF, M.Z., Observations on the adequacy of some transport and activation cross-sections as revealed from the integral experiments of the US/JAREI Collaborative Program on Fusion Neutronics, and other papers presented at the IAEA Advisory Group Meeting on FENDL-2 and Associated Benchmark Calculations, Nov. 18-22, 1991, Vienna, Austria.

[4] Materials of the IAEA Advisory Group Meeting on FENDL-2 and Associated Benchmark Calculations, Nov. 18-22, 1991, Vienna, Austria. Report INDC (NDS)-260, Vienna (1992).

[5] SAL'NIKOV, O.A., LOVCHIKOVA, G.N., KOTEL'NIKOVA, G.V., et al., in Problems of Atomic Science and Technology, Ser. Nuclear Constants 7 (1972) 102, 134 (in Russian).

[6] IGNATYUK, A.V., LUNEV, V.P., Report NEANDC-245 'U' (1988).

[7] ENDF-102 Data Formats and procedures for the Evaluated Nuclear Data File ENDF-6, Report BNL-NCS-44945, (Rose, P.F. and Dunford, C.L., Eds) (1990).

[8] FISHER, U., SCHWENK-FERRERO, A., WIEGNER, E., Analyses of 14 MeV neutron transport in beryllium; FISHER, U. and WIEGNER, E., ^{56}Fe benchmark calculations with EFF-2 and ENDF/B-VI DDX-data: An Interim Report, see [4].

[9] SIMAKOV, S.P., DEVKIN, B.V., KOBOZEV, M.G., et al., Leakage neutron spectra from Al, Fe, Ni and U spheres with 14 MeV and ^{252}Cf neutron sources, see Ref. [4].

[10] ANDROSENKO, A.A., ANDROSENKO, P.A., et al., in Problems of Atomic Science and Technology, Ser. Nuclear Constants 7 (1985) 33 (in Russian).

[11] ENGL, W.W., A user's manual for ANISN. A one-dimensional discrete ordinate transport code with anisotropic scattering, K-1693, Union Carbide Corporation, Computing Technology Center (1976).

[12] KALBACH, C., Phys. Rev., 37 (1988) 2350.

[13] WILLIAMS, M.L., Impact of iron cross-section evaluations on calculated neutron transmission through steel, Attachment 4C-6 in the Summary of the CSEWG Meeting, May 8-10, BNL, USA (1991).

[14] KOLEVATOV, Yu.I., TRYKOV, L.A., in Third All-Union Conference on Protection of Nuclear Facilities from Ionizing Radiation, Abstracts of papers, Tbilisi, Inst. Appl. Math., Tbilisi State Univ. (1981) 95 (in Russian).

[15] GLUKHOVETS, N.A.., FILIPPOV, V.V., Nejtronnaya fizika 4 (1980) 15.

[16] FILIPPOV, V.V., in Problems of Atomic Science and Technology, Ser. Nuclear Constants 3 (1987) 30 (in Russian).

[17] ANDROSENKO, A.A., ANDROSENKO, P.A., DEVKIN, B.V., et al., Kernenergie 31 10 (1988) 122.

[18] MUGHABGHAB, S.F., DIVADEENAM, M., HOLDEN, N.E., Neutron Cross Sections, Vol. 1: "Neutron Resonance Parameters and Thermal Cross Sections", Academic press, New York (1981).

[19] HERTEL, N.E., Fusion Technology 9 (1986) 345.

TABLE 1. CHARACTERISTICS OF SPHERES USED IN THE CALCULATIONS

Material, reference	Density with respect to the basic material	Radius of sphere, cm		Radius of channel, cm	Allowance for impurities
		Internal	External		
Beryllium [17]		6.0	11.0	2.5	No
Iron [9]		4.5	12.0	3.1	No
Iron [19]	7.87	7.65	38.1		No

TABLE 2. ANGLE-ENERGY DISTRIBUTIONS AND SOURCE NEUTRON YIELDS PRESENTED IN THE FORM OF A HISTOGRAM

Interval of angles in the scale, cos (θ)	Source neutron energy interval, MeV	Neutron yield, I/d (cos(θ))
-1.0 - -0.8	13.358 - 13.504	0.09516
-0.8 - -0.6	13.504 - 13.651	0.09626
-0.6 - -0.4	13.651 - 13.800	0.09726
-0.4 - -0.2	13.800 - 13.951	0.09840
-0.2 - 0.0	13.951 - 14.103	0.09942
0.0 - 0.2	14.103 - 14.257	0.10050
0.2 - 0.4	14.257 - 14.413	0.10160
0.4 - 0.6	14.413 - 14.571	0.10270
0.6 - 0.8	14.571 - 14.730	0.10381
0.8 - 1.0	14.730 - 14.891	0.10496

TABLE 3. PARTIAL NEUTRON LEAKAGES FROM A BERYLLIUM SPHERE, Δd = 5 cm

Neutron energy, MeV	Experiment, [17]	Calculation using BRAND (^{56}Fe, ENDF/B-6)	
		With allowance for anisotropy in the "continuum"	Without allowance for anisotropy in the "continuum"
0.4 - 1.0	0.12	0.094	0.095
1.0 - 3.0	0.157	0.137	0.131
3.0 - 10.0	0.178	0.161	0.148
10.0 - 15.0	0.690	0.730	0.716

TABLE 4. PARTIAL NEUTRON LEAKAGES FROM AN IRON SPHERE, Δd = 7.5 cm

Neutron energy, MeV	FEhI experiment [9]	IAEh experiment [20]	Calculation	
			BRAND (ENDF/B-6)	ANISN (S16P11) (BROND)
1.0 - 5.0	0.295	0.362	0.244	0.272
5.0 - 10.0	0.0492	0.05	0.029	0.0396
10.0 - 15.0	0.511	0.427	0.364	0.448
1.0 - 15.0	0.8552	0.839	0.637	0.7596

FEhI = Institute of Physics and Power Engineering, Obninsk
IAEh = I.V. Kurchatov Institute of Atomic Energy

TABLE 5. PARTIAL NEUTRON LEAKAGES FROM AN IRON SPHERE, Δd = 30.45 cm

Neutron energy, MeV	Experiment [19]	Calculation ANISN (S16P11) (BROND)
1.0 - 2.2	0.19 ± 0.01	0.0657
2.2 - 5.0	0.023 ± 0.001	0.0184
5.0 - 10.0	$(5.3 \pm 2.2) \cdot 10^{3}$	$7.4 \cdot 10^{-3}$
10.0 - 15.0	0.02 ± 0.001	0.0396
2.2 - 15.0	0.0483	0.065

Note: Partial neutron leakages are the number of neutrons per source neutron in the given energy interval.

TABLE 6. PARTIAL NEUTRON LEAKAGES IN THE ENERGY INTERVAL 0.4-0.8 MeV FOR AN IRON SPHERE WITH Δd = 30.45 cm FOR DIFFERENT GROUPINGS WITHIN THIS INTERVAL

Number of groups	Width of group, keV	Calculation ANISN (S16P11) (BROND)
1	400	0.196
7	~60	0.224
20	20	0.255
80	5	0.271
1	400*	0.326

* With allowance for self-shielding.

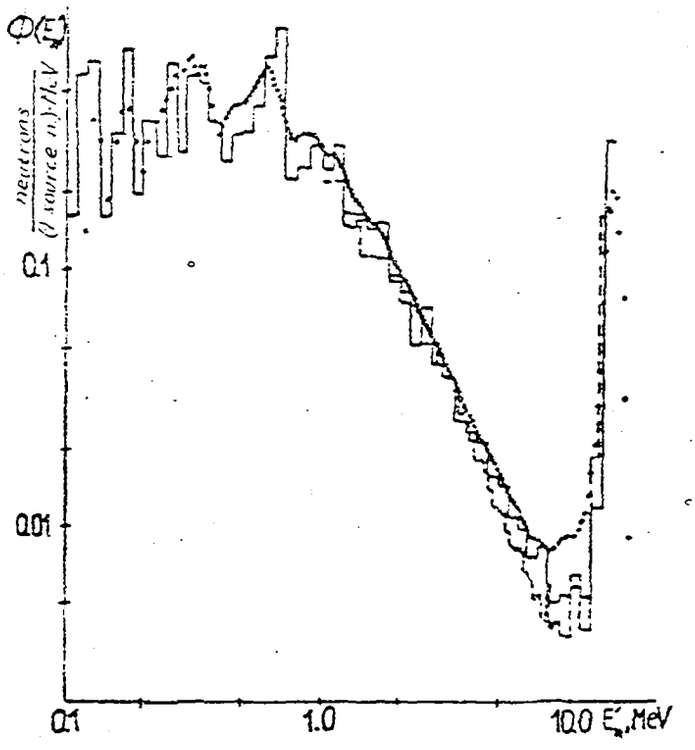

FIG. 1. Leakage neutron energy spectrum for an iron sphere with Δd = 7.5 cm. The points represent experimental data [9], the broken line the results of calculation by the Monte Carlo method with the BRAND program for ^{56}Fe from the ENDF/B-6 library, and the solid line the results of calculation by the discrete ordinates method with the ANISN program in the S16P11 approximation for ^{nat}Fe from the BROND library.

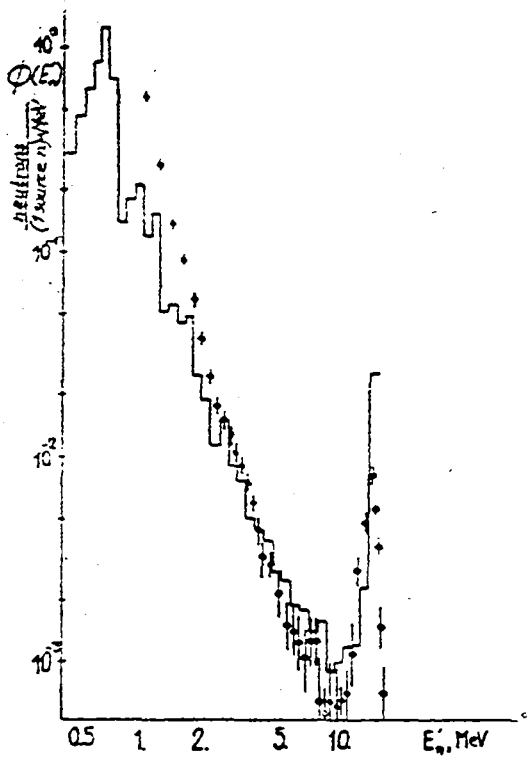

FIG. 2. Energy spectrum of leakage neutrons for an iron sphere with $\Delta d = 30.45$ cm. The points represent experimental data [19] and the solid line the results of calculation by the discrete ordinates method with the ANISN program in the S16P11 approximation for ^{nat}Fe from the BROND library.

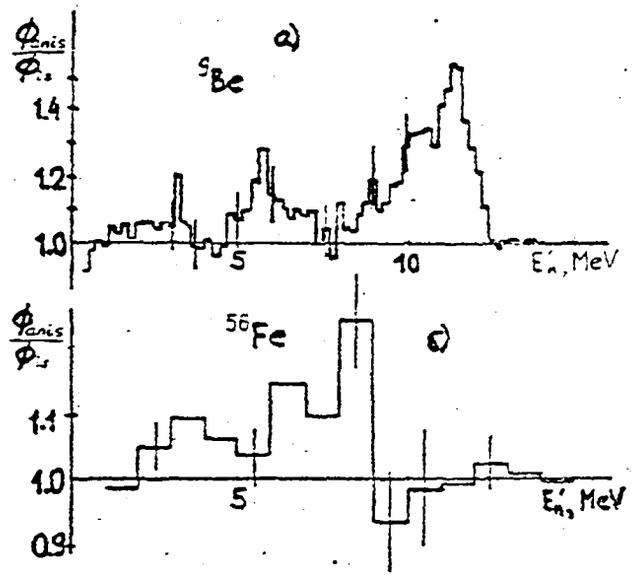

FIG. 3. Ratio of the leakage spectra calculated with allowance for anisotropy in the angular distributions of inelastic processes to the same spectra without such allowance (a) for a beryllium sphere with $\Delta d = 5$ cm and (b) for an iron sphere with $\Delta d = 7.5$ cm. In the calculations by the Monte Carlo method the ENDF/B-6 library files for ^{9}Be and ^{56}Fe were used. The statistical errors of the calculations are indicated.

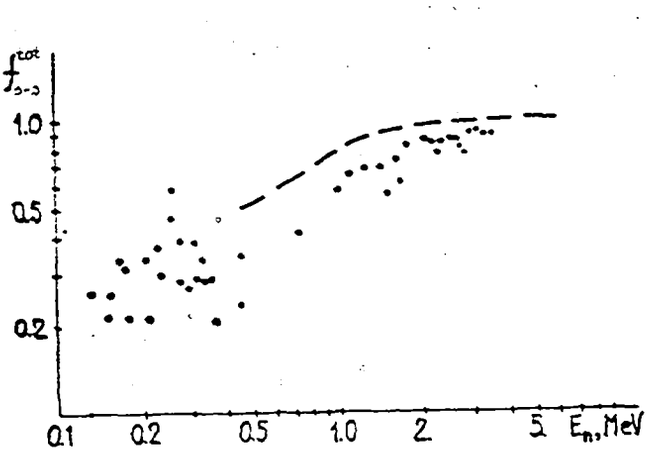

FIG. 4. Self-shielding factors of iron cross-sections from Ref. [15]. The points represent experimental data from measurements for transmission in thick specimens and the broken line the results of calculation from experimental data (point curves of cross-sections), measured with high resolution.

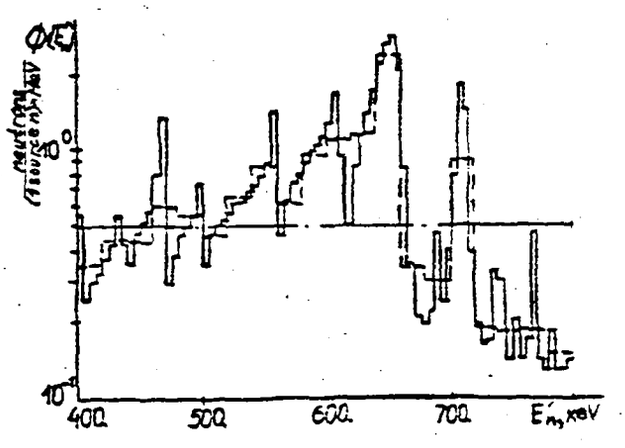

FIG. 5. Neutron leakage spectra from an iron sphere with Δd = 30.45 cm in calculations using the ANISN program with different groupings in the 400-800 keV energy interval. The solid line represents 80 groups and the broken line 20 groups.

95-11660 (H+)
Translated from Russian

EVALUATION OF NEUTRON CROSS-SECTIONS OF ^{127}I IMPORTANT FOR RADIATION TRANSPORT CALCULATIONS IN LARGE NaI DETECTORS

V.G. Proynaev
Institute of Physics and Power Engineering
(State Scientific Centre of the Russian Federation), Obninsk

ABSTRACT

Evaluations were made of neutron inelastic scattering cross-sections with excitation of discrete levels of the residual nucleus, the (n,2n) reaction, secondary neutron emission spectra and secondary photons for reactions which contribute substantially to production of photons for ^{127}I with the use of the theoretical model for neutrons with an initial energy of 60 keV-20 MeV.

INTRODUCTION

The evaluated neutron cross-section files for ^{127}I available in the ENDF/B, JENDL and JEF libraries are part of the evaluated data libraries for fission products and, as they are incomplete, do not contain all the data required to calculate neutron and gamma-ray transport in media containing iodine. At the same time a knowledge of these nuclear data is essential for calculating the sensitivity of large NaI detectors to neutrons in a broad energy range. In order to fill this gap, we have used the TNG code [1], which is based on statistical and pre-equilibrium models of nuclear reactions, for calculations of secondary particle cross-sections and spectra for main neutron- and gamma-producing channels for the interaction between neutrons with an energy from 60 keV to 20 MeV and ^{127}I.

EVALUATION METHOD AND SELECTION OF MODEL PARAMETERS

Since, unlike that of main structural and fissile materials, the experimental database for the monoisotope ^{127}I is extremely incomplete and contradictory, we used a theoretical model to evaluate method based on the TNG code [1], which was developed at the ORNL specially for the evaluation of neutron cross-sections and their presentation in the ENDF format. In the neutron energy range up to 20 MeV, the main cross-sections leading to the emission of secondary neutrons and photons are neutron inelastic scattering, the (n,2n) reaction and the neutron radiative capture reaction. All other reactions (apart from the total cross-section and the (n,3n) cross-section) were considered to be minor and their evaluation was taken from the evaluated file for iodine from the JEF-2 fission product library. The (n,3n) cross-section, which is significant at the neutron energy 25 MeV, was taken from the JENDL-2 fission product library. The MF = 2 file from the JEF-2 library was used for evaluation of cross-sections in the resonance region of neutron energies ($E < 60$ keV).

All calculations of cross-sections and angle energy distributions of secondary particles for neutrons with an initial energy from 60 keV to 20 MeV were performed with the potential parameters [2] of the spherical optical model. In order to describe the level density in all channels with a continuous level spectrum, we used the temperature approximation in the Gilbert-Cameron parametrization [3]. The positions, spins, and parities of discrete levels in the inelastic scattering and (n,2n) reaction channels as well as the probabilities of gamma transitions between discrete levels were taken from the evaluated data file for the nuclear structure [4], and the beginning of the level continuum coincided with the excitation energy at which the level gap became noticeable. The criterion for the reliability of the calculations was in all cases agreement with existing experimental data.

As the physical processes were known to be inappropriate for the models used, the model parameters had to be deformed to describe the cross-sections. Thus, in the level density formula in the Gilbert-Cameron parameterization, the spin dependence parameter in all channels was taken as 1.3 instead of the recommended value of 4.3. Since consideration of competition between neutron and gamma channels is limited in the TNG by two-stage processes, whereas processes of the form (n,n'γn), which contribute to the (n,2n) reaction are not taken into account, it is necessary artificially to reduce the cross-section at the maximum of the giant dipole resonance when calculating the gamma widths in order to describe the (n,2n) cross-section near the threshold. This change has an effect to some degree on the shape of the secondary photon spectra.

As already noted, only the main partial reactions which make a major contribution to the cross-sections for the production of secondary neutrons were considered explicitly. All other minor reactions were taken from earlier evaluations and considered in the calculations on the level of balance ratios. In order to take into account the contribution of direct processes to inelastic scattering with excitation of discrete levels, we performed calculations, using the ECIS87 program [5], of the contribution of the direct process for inelastic scattering with excitation of states of the multiplet ($1/2^+$, $3/2^+$, $5/2^+$, $7/2^+$, $9/2^+$) constructed in the model for weak coupling between a single-photon excitation 2^+ in the ^{126}Te nucleus (NUCLEAR CORE) and a proton located at the single-particle level $3d_{5/2}$. The same optical potential parameters [2] as in the TNG code and the root-mean-square parameter of dynamic deformation $\beta_\lambda = 0.16$ [4] were used in the calculation.

To reduce the uncertainty in the evaluation of spectra for secondary photons limited during neutron radiative capture, the results of spectrum shape measurements performed in Ref. [6] for neutrons with an initial energy of 500 keV, supplemented with normalized strong

discrete gamma-transitions, were taken as evaluated values. Knowing the total energy release in the radiative capture channel and the mean spectrum energy, we can obtain an evaluation of the multiplicity of neutrons at this energy. Neglecting the change in the spectrum shape with increase in neutron energy, which is valid to some extent if we neglect the contribution of direct-semi-direct capture, we associate the change in total energy release with the change in the multiplicity of secondary photons in the radiative capture channel. The cross-section from the JEF-2 fission product data library was taken as the evaluation for the radiative capture cross-section.

EVALUATION RESULTS AND COMPARISON WITH EXPERIMENTAL DATA

Although this approach to evaluation, which concentrates on those cross-sections and secondary-particle distributions that basically determine the accuracy of calculations of neutron and photon transport in fields generated by fission spectrum neutrons, is approximate, it is entirely satisfactory for the given application. Figure 1 shows a comparison of experimental data [7] for 58 keV photon production cross-section (gamma transition between the first excited state and the ground state) with the present calculation results. It should be noted that the complete experimental database for secondary photon yield is extremely inconsistent. At the same time the calculation results for photon formation cross-sections for inelastic neutron scattering near the threshold of the level from which the gamma decay under study takes place depend substantially on the behaviour of the optical potential at low neutron energies. Therefore, in order to improve the description of cross-sections near the threshold, we have to do without global parameterization and perform a more detailed study of the properties of the optical potential for a given nucleus at low neutron energies.

The calculations of the 203 keV photon yield cross-sections corresponding to the transition between the level with an excitation energy of 203 keV and the ground state are shown in Fig. 2 in comparison with experimental data [8]. We note that in this case agreement between calculation and experiment is sufficiently good.

All cross-section calculations were performed with allowance for a correction for neutron width fluctuation. Applying the correction for the correlation of neutron widths may improve the agreement between the calculations and the experimental data shown in Fig. 1 for higher energies.

The (n,2n) cross-section calculation results are shown in Fig. 3 in comparison with all available experimental data [9]. A satisfactory description was obtained by varying the two basic parameters: the cross-section at the maximum dipole resonance, the selection of which mainly affects the behaviour of the (n,2n) cross-section near the reaction threshold, and the magnitude of the contribution of pre-equilibrium processes determining the cross-section at the maximum. The decrease in the (n,2n) cross-section has been caused mainly by competition from the (n,3n) channel, which is taken into account in the calculations by means of the cross-section balance. One disadvantage of this description is that the secondary neutron emission spectrum calculated in the pre-equilibrium decay model used here is not sufficiently hard, leading to a distortion in the shape of the (n,2n) and (n,n'γ) reaction excitation functions. The secondary photon spectra for all reactions which do not make a noticeable contribution to the total gamma production cross-section were presented in the simplest temperature form.

CONCLUSION

The ^{127}I file from the JEF-2 fission product library was reviewed and supplemented with the angle-energy distributions of secondary particles so that it could be used to calculate neutron and gamma-radiation transport in a large NaI detector.

REFERENCES

1. Fu C.Y., Shibata K.: Computer Code TNG: ORNL, 1988, private communication.
2. Wilmore D., Hodgson P.E.//Nucl.Phys. 1964. V.55. P.673.
3. Gilbert A., Cameron A.G.W.//Canad.J.Phys. 1965. V.43. P.1446.
4. Evaluated Nuclear Stucture Data File. Data Base on 1991.
5. Raynal J.: Computing as a Language of Physics. 1972. IAEA. Vienna. P.281.
6. Voignier J., Joly S., Grenier G.//Nucl.Sci.Eng. 1986. V.93. P.43.
7. Bain C.A., Brooks F.D.//Nucl.Phys. 1986. V.A125. P.312.
8. Lind D.A., Day R.B.//Ann.Phys. 1961. V.12. P.856.
9. EXFOR - Exchange Format. Data Base on 1994.

[10] Manokhin, V.N., Problems of Atomic Science and Technology, Ser. Nuclear Constants, No. 1 (1994) 18 (in Russian).

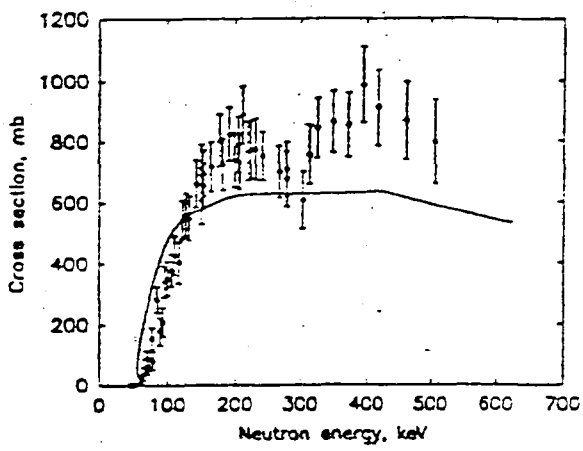

FIG. 1. Comparison of the results of calculation of the 58 keV photon yield cross-section (solid line) with experimental data [7] (solid circles).

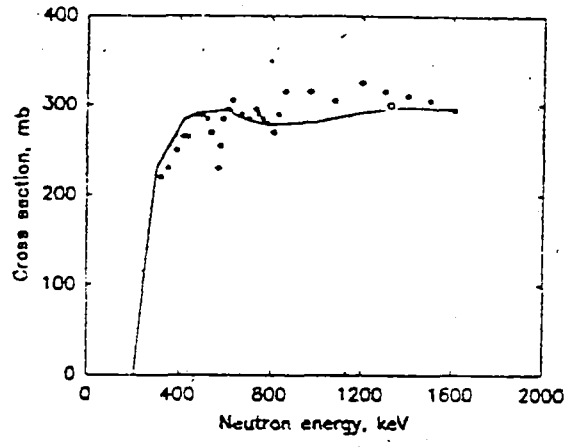

FIG. 2. Comparison of the results of calculation of the 203 keV photon yield cross-section (solid line) with experimental data [8] (solid circles).

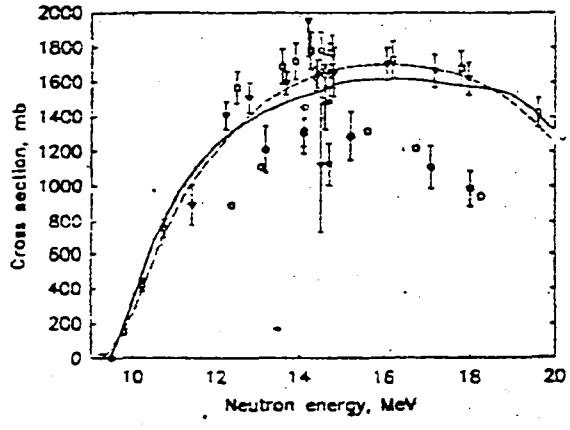

FIG. 3. Comparison of the results of calculation of the (n,2n) cross-section obtained in the present work (solid line) with available experimental data taken from the EXFOR library [9] and the curve obtained by parametrization of the shape of the energy dependence of the (n,2n) cross-section (dashed line) [10].

95-11660 (32 + H)
Translated from Russian

UDC 539.172

EVALUATION OF $^{23}Na(n,2n)^{22}Na$ REACTION CROSS-SECTIONS

V.N. Manokhin

Institute of Physics and Power Engineering
(State Scientific Centre of the Russian Federation)
Obninsk

ABSTRACT

Using available experimental data and (n,2n) excitation function systematics $^{23}Na(n,2n)^{22}Na$ reaction cross-sections were evaluated for energies ranging from the reaction threshold to 20 MeV.

The $^{23}Na(n,2n)^{22}Na$ reaction is of interest for determining neutron fluence in fission and fusion reactors. Furthermore, this reaction is of interest because of the need to estimate the production of ^{22}Na, which has a long half-life (2.60 years) and can accumulate in sodium-cooled fast breeder reactors. This reaction is also important in connection with the development of low-activated materials in fusion devices since ^{22}Na can be produced in the $^{27}Al(n,n\alpha)^{23}Na(n,2n)^{22}Na$ and $^{23}Mg(n,np)^{23}Na(n,2n)^{22}Na$ reactions.

It should be noted that sodium occurs as an impurity in lithium and, for the hard spectrum and intensive neutron flux in fusion devices, there will be a build-up of ^{22}Na as a result of the $^{23}Na(n,2n)$ reaction.

Two evaluations of the $^{23}Na(n,2n)^{22}Na$ reaction are currently available: ENDF/B-6 [1] and JENDL-DOS [2], but they differ markedly. Further measurements, analysis and evaluation of the cross-sections of this reaction are therefore required.

As a whole the available experimental data cover the entire energy range from the reaction threshold (12.958 MeV) to ~ 20 MeV and are shown on Fig. 1. As can be seen, there are large differences between the data of the various authors in the neutron energy range above ~ 14.5 MeV. The data divide into two groups which at energies greater than 16 MeV differ by approximately a factor of 2.

Larson's comparative analysis [1] of the measurement results presented in a number of papers (including Refs [3-6]) did not provide sufficient justification for disregarding the data of Prestwood [3], whose was the only paper in the upper group until the publication in 1991 of Xu and Pan's paper [16] with similar results. It should be noted that in both of these papers ^{22}Na activity was measured on the basis of annihilation photons with an energy of 511 keV. In Ref. [15] Strohmaier measured ^{22}Na activity on the basis of the 1274.5 keV gamma line, compared the result obtained with the annihilation photon measurements and obtained good agreement. In their view Refs [4, 16] may contain a systematic error in the recording of the 511 keV annihilation radiation. In Ref. [16], too, a theoretical analysis of the $^{23}Na(n,2n)$ reaction excitation function was made. It is shown that the theoretical excitation function of this reaction lies approximately in the middle of the two groups of measurement in the 18-20 MeV neutron energy region and closer to the upper group at 15-18 MeV.

The data of Sakuma et al. and Uno et al. [19, 20], as we can see from the figures, lie in the lower measurement group.

Large differences in the experimental data have resulted in equally large differences in evaluations. The ENDF/B-6 evaluation is close to the upper group, which includes the experimental data from Refs [4, 16]. The JENDL-DOS evaluation [2] is close to the lower group of measurements.

The present paper proposes an evaluation based on the data for the lower measurement group and, principally, the results given in Refs [13, 15, 18]. The evaluation was carried out by approximating the energy dependence of the reaction cross-section with the help of the normalized (n,2n) reaction excitation function obtained in Ref. [21] on the basis of comparison of experimental excitation functions. The parameters for this function are given in Table 1.

$\Delta E = E_n - E_{th}$, where E_n is the neutron energy and E_{th} the threshold energy; σ_{max} is the (n,2n) reaction cross-section at the maximum of the excitation function at an energy above the reaction threshold ΔE_{max}, determined in the limiting case as $(E_{th}^{n,3n} - E_{th}^{n,2n})$. Since the (n,2n) reaction cross-section at approximately 7 MeV more or less reaches a plateau and shows no noticeable change within a range of several MeV, there is uncertainty in selecting the value of ΔE_{max} in cases where the difference in the thresholds of the two reactions mentioned above is greater than 7-8 MeV. Therefore, some variation in this value is permissible in order to obtain an optimal description of the available experimental data and/or to satisfy the requirements of the cross-section systematics.

When evaluating the $^{23}Na(n,2n)^{22}Na$ reaction cross-section the following values were taken: $\Delta E_{max} = 8.0$ MeV, $\sigma_{max} = 115$ mb. This enabled good agreement to be obtained between the calculated excitation function and the data in Refs [13, 15, 18]. Table 2 gives the numerical values of the evaluated excitation function.

When determining the errors of the evaluated data allowance was made for error in σ_{max} and in determination of the shape of the normalized function.

The following errors for the evaluated cross-sections are recommended:

13.0-13.5 MeV	20%	15.0-18.0 MeV	7%
13.5-14.0 MeV	15%	18.0-20.0 MeV	5%
14.0-15.0 MeV	10%		

Since the $^{23}Na(n,2n)^{22}Na$ reaction threshold is high (12.958 MeV) and the intensity of neutrons with an energy above 13 MeV in the ^{235}U and ^{252}Cf fission spectrum is low, the cross-section averaged over these spectra makes it impossible to choose between the two measurement groups mentioned earlier.

In Ref. [17] Dumais et al. used measurements in the neutron field from the Li(d,n) reaction on a thick target to test the cross-sections in the region from the threshold to ~ 16 MeV. There is a relatively high proportion of neutrons with an energy above the (n,2n) reaction threshold in the spectrum of neutrons from this reaction. Comparison of the calculated and experimental results showed that the ENDF/B-6 data, which are based on the measurements in Ref. [4], are excessively high (50%). The JENDL-DOS data, on the other hand, give a cross-section value, calculated from the Li(d,n) reaction neutron spectrum, which is 10-15% lower than the experimental integral value. All this points in favour of the microscopic cross-sections in the lower group of measurements. The evaluation given in this paper is close to the JENDL-DOS evaluation and it does not conflict with the integral measurements in Ref. [17].

REFERENCES

1. Larson D. Nucl.Sci.Eng. 78, 324 (1981).
2. JENDL Dosimetry File. Report JAERI-1325, 1992.
3. Prestwood R.J. Phys.Rev., 98, 47 (1955).
4. Picard J., et al. Williamson Nucl.Phys., 63, 673 (1965).
5. Liskien H., Paulsen A. Nucl.Phys., 63, 393 (1965).
6. Menlove H.O. et al. Phys.Rev., 163, 1308 (1967).
7. Barrall R.C. et al. Report AFWL-TR-68-134 (1968).
8. Araminowicz J. et al. Report INR-1464/I/A/*, 14 (1973).
9. Maslov G.N. et.al. Report YF-9, 50 (1972).
10. Shani G. Report INIS-MF-3663, 83 (1976).
11. Sigg R.A. Thesis. Univ. of Arkansas (1976).
12. Adamski L. et al. Ann.Nucl.Energy, 7, 397 (1980).
13. Ikeda Y. et al. Report JAERI-1312 (1988).
14. Wagner M. et al. IRK Progress Report, 15 (1990).
15. Strohmaier B., Wagner M., Vonach H. In: Proc.of Conf. on nucl. Data for Science and Techn., Juelich, Germany, 1991, p.663.
16. Xu Zhi-Zheng, Pan Li-Min Ibid, p.666.
17. Dumais J.R. et al. Ibid, p.202.
18. Lu Hanlin, Zhao Wenrong, Yu Weixiang Chi. J.Nucl.Phys., 14, 83 (1992).
19. Sakuma M. et al. In: Proc. of the 1991 Symp. on Nucl.Data, JAERI-M 92-027 (1992), p.278.
20. Uno Y. et al. In: Proc. of the 1992 Symp. on Nucl. Data, JAERI-M 93-046 (1993), p.247.
21. Manokhin, V.N., in: Problems of Atomic Science and Technology, Ser. Nuclear Constants No. 1 (1994) 18 (in Russian).

TABLE 1: NORMALIZED EXCITATION FUNCTION OF THE (n,2n) REACTION

$\Delta E/\Delta E_{max}$	σ/σ_{max}	$\Delta E/\Delta E_{max}$	σ/σ_{max}
0.05	0.03	0.50	0.81
0.10	0.09	0.55	0.85
0.15	0.18	0.60	0.88
0.20	0.30	0.65	0.91
0.25	0.42	0.70	0.93
0.30	0.53	0.75	0.95
0.35	0.60	0.80	0.97
0.40	0.68	0.85	0.98
0.45	0.75	0.90	0.99

TABLE 2: EVALUATED CROSS-SECTIONS FOR THE $^{23}Na(n,2n)^{22}Na$ REACTION

E_n, MeV	σ, mb	E_n, MeV	σ, mb
13.0	0	17.0	90.0
13.5	5.0	17.5	96.0
14.0	15.0	18.0	101.0
14.5	32.0	18.5	105.0
15.0	50.0	19.0	108.0
15.5	63.0	19.5	110.0
16.0	73.0	20.0	112
16.5	82.0		

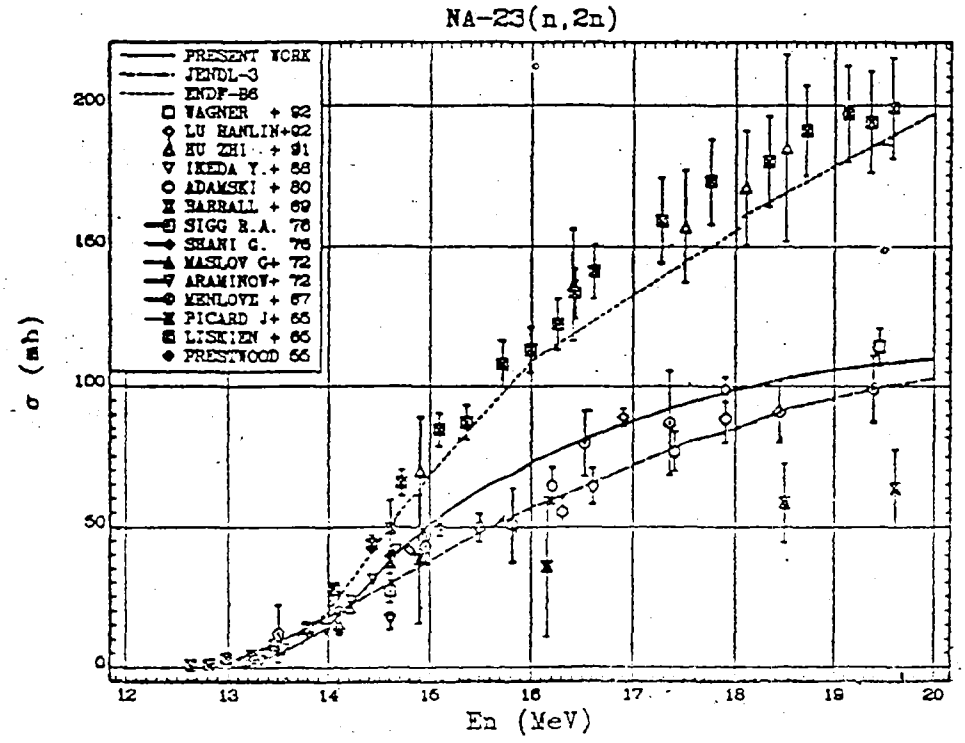

FIG 1: $^{23}Na(n,2n)^{22}Na$ cross-section.

95-11660 (32 + H)
Translated from Russian

UDC 621.039.51

MEASUREMENT OF GAMMA-RAY MULTIPLICITY SPECTRA AND THE ALPHA VALUE FOR ^{235}U RESONANCES

Yu.V. Grigor'ev
Institute of Physics and Power Engineering, Obninsk

G.P. Georgiev and Kh. Stanchik
Joint Institute for Nuclear Research, Dubna

ABSTRACT

Gamma spectra from 1 to 12 multiplicity were measured on the 500 m flight path of the IBR-30 reactor using a 16-section 32 L NaI(Tl) crystal scintillation detector able to hold 2 metallic samples of 90% ^{235}U and 10% ^{238}U 0.00137 atoms/b and 0.00411 atoms/b thick. Multiplicity spectra were obtained for resolved resonances in the E = 1-150 eV energy region. They were used to determine the value of $\alpha = \sigma_\gamma/\sigma_f$ for 165 resonances of ^{235}U.

Introduction

The multiplicity spectra of ^{235}U gamma-rays were measured earlier in the energy resonance region [1, 2] and on thermal neutrons [3] with a view to determining the fission and radiative capture cross-sections and the value of $\alpha = \sigma_\gamma/\sigma_f$. These measurements showed that use of the radiation multiplicity spectrometry could reduce methodological errors due to backgrounds and normalization to reference values. A positive feature of this method is that in a single experiment several nucleus excitation processes can be observed at the same time. However, the radiation multiplicity spectrometry method is not yet in general use, evidently because of its complexity and the high cost of the equipment used. The present work is an

attempt to use radiation multiplicity spectrometry during excitation of ^{235}U nuclei by resonance neutrons in order to study the shape of the gamma-ray multiplicity spectra during fission and radiative capture, and also to improve the accuracy of some of the constants used in reactor calculation.

Experimental method

The ^{235}U gamma-ray multiplicity spectra were measured on the 500 m flight path of the IBR-30 reactor using a 16-section scintillation detector with NaI(T1) crystals having a total volume of 32 L [4]. During the measurements the IBR-30 pulsed fast reactor operated in two modes - at an average thermal power of 10 (5) kW, with a neutron burst repetition frequency of 100 (25) Hz and a burst duration of 4 μs at half-height. Metallic discs made of uranium with a 90% ^{235}U and 10% ^{238}U content were used as radiator samples. The samples were packed in 0.15 mm thick aluminium foil. The sample diameter was 45 mm, the thickness 0.00137 nuclei/b, and the weight of each sample was approximately 8 g. The samples were fixed in the middle of the detector in a vacuum tube. During operation of the neutron source at 10 kW four samples were placed in the detector in a single plane; at 5 kW the radiator sample was in the form of a sandwich made up of three discs with a total thickness of 0.00411 nuclei/b.

The beam was passed through a 10 mm thick boron carbide filter [was attached to the beam] for the 100 Hz neutron burst frequency or through a 1 mm cadmium sheet filter for the 25 Hz frequency to remove background recycling neutrons. In addition, manganese and cobalt resonance filters were fitted on the beam to determine the background components in the time spectra. To reduce the neutron fission background and to record the process of neutron scattering on the sample cylindrical converters of borated polyethylene 35 mm thick and of ^{10}B 10 mm thick were mounted inside the detector. The discrimination levels in each

detector channel corresponded to a 100 keV energy release. After the linear adder for signals from all 16 channels the discrimination window discriminated pulses corresponding to an energy release in the range 2-10 MeV. The discrimination window for neutrons scattered by the sample was selected to be 400-600 keV. Information in the form of 16 time spectra, covering the 15 eV-10 MeV neutron energy range was stored in the interim memory of the measuring module using a Pravets-16 personal computer. The first 12 spectra corresponded to coincidence multiplicities from 1 to 12 for radiative capture and fission, spectra 13 and 14 contained information on neutron scattering by the sample in the first and second half of the detector, and spectra 15 and 16 were used for auxiliary purposes. The typical instrument time spectra of the different multiplicities without and with deduction of the background are shown in Figs 1 and 2.

Measurement results

From the experimental time spectra after deduction of background components we obtained the coincidence multiplicity spectra from the first to the eleventh multiplicity for 165 resonances in the E = 150 eV region. They were normalized to unity and are shown on Figs 3-6. The shape of the multiplicity spectra for resonances with small fission widths (Fig. 3) differ considerably from the shape of the spectra with large fission widths (Fig. 4). Thus, the resonance at energy 94.1 eV with an anomalously small fission width Γ_f = 0.2 MeV has an average multiplicity K_{av} = 3.04, while the resonance at energy 44.86 eV with a maximum width Γ_f = 660 MeV has K_{av} = 4.38, i.e. the first resonance is actually a capture resonance and the second a fission resonance. These resonances were used to divide the multiplicity spectra of the other resonances into two components: fission and radiative capture processes. When dividing the initial multiplicity spectra the first and second multiplicities, where actually no fission occurs, were used as reference multiplicities for

generating the capture spectrum, and multiplicities above the sixth, where there is no radiative capture, were used to obtain the fission part of the spectrum. By way of example this division is shown on Figs 5 and 6 for resonances at energies 44.6 eV (Γ_γ = 35 MeV, Γ_f = 170 MeV) and 72.4 eV (Γ_γ = 35 MeV, Γ_f = 98 MeV). Both resonances have a spin of J = 4. The average multiplicities for the fission spectra for these resonances coincided and were equal to K_{fav} = 5.32. The change in the shape of the sum multiplicity spectra as a function of the resonance fission widths can be judged from Fig. 7, which shows the average multiplicities of the sum spectra as a function of Γ_f. The increase in K_{av} as Γ_f increases is explained by the rise in the sum spectrum of the share of the fission process where more photons are emitted as compared with radiative capture.

Division of the sum multiplicity spectra into two parts enables us to determine the alpha value:

$$\alpha = \sigma_\gamma / \sigma_f = N_\gamma \varepsilon_f / N_f \varepsilon_\gamma = \Sigma K_{i\gamma} / \Sigma K_{if} \varepsilon_\gamma ,$$

where σ_γ, σ_f are the radiative capture and fission cross-sections, N_γ, N_f the total number of capture and fission photon counts, ε_γ, ε_f the efficiency of recording capture and fission photons; and, $K_{i\gamma}$, K_{if} the i-th multiplicity of radiative capture and fission.

Assuming that the photon recording efficiency is not energy-dependent, the ratio $Q = \varepsilon_f/\varepsilon_\gamma$ can be determined by normalization to the alpha values obtained in the precision measurements contained in Ref. [2]. The errors in the alpha value depend mainly on errors in resolution of the sum multiplicity spectra into their fission and radiative capture components. Errors due to uncertainties in the photon recording efficiencies are considerably lower since $Q = \varepsilon_f/\varepsilon_\gamma$ is close to unity. As a result of the normalization of alpha for 13 resonances in this experiment and in Ref. [2], the ratio of efficiencies obtained was 1.033. The experimental alpha values are given in Table 1. For comparison purposes we also give

the data of Refs [2, 5]. As can be seen from the table, the alpha values obtained for some resonances differ considerably from the data in the other papers [2, 5], and this is possibly due to the different energy averaging intervals.

The experimental errors for the alpha values in the present work are 3-7%, and for large and small alpha values the errors are as high as 10%. As follows from the table, division of the average multiplicities according to resonance spins is not observed in the given experiment but there is a periodic dependence of K_{av} on energy, the minima of which are associated with small fission widths Γ_f of the resonances.

Conclusion

Thus, the extensive experimental material presented in this paper points to the great potential of radiation multiplicity spectrometry of excited fissioning nuclei. The alpha determination method is more accurate than those considered in Ref. [6] and have been in use so far. The results of the present work do not confirm the assumption about spin dependence of average radiation multiplicities for resolved resonances. It is advisable in future to continue investigations in this area using different fissioning isotopes.

REFERENCES

[1] MURADYAN, G.V., USTROEV, G.I., SHCHEPKIN, Yu. G., et al., "Measurement of fission and capture cross-sections and alpha of uranium-235", Proc. 4th All-Union Conference on Neutron Physics, Kiev, 18-22 April 1977, Vol 3, Moscow (1977) 119 [in Russian].

[2] ADAMCHUK, Yu.V., VOSKANYAN, M.A., MURADYAN, G.V., et al., "Measurement of the alpha value on ^{235}U and ^{239}Pu resonances", Proc. 6th All-Union Conference on Neutron Physics, Kiev, 2-6 October 1983, Vol. 2, Moscow (1984) 137 [in Russian].

[3] GEORGIEV, G.P., Measurement of the Alpha Value of Uranium-235 on Thermal Neutrons, Author's Abstract of Doctoral Thesis, Sofia (1986) [in Russian].

[4] JANEVA, N., TOSHKOV, S., MURADYAN, G.V., et al., A setup for precise measurement of resonance neutron capture by self-indication. Nucl. Instrum. Methods Phys. Res. A313 (1992) 266.

[5] GWIN, R., SILVER, E.G., INGLE, R.W., WEAVER, H., Measurement of the neutron capture and fission cross sections of ^{239}Pu and ^{235}U, 0.02 eV to 200 keV, the neutron capture cross sections of ^{197}Au, to 50 keV, and neutron fission cross sections of ^{233}U, 5 to 200 keV, Nucl. Sci. Eng. 59 (1976) 79.

[6] VAN'KOV, A.A., GRIGOR'EV, Yu.V., Classification of Methods to Measure the Neutron Capture to Fission Cross-Section Ratio, Preprint FEhI-325, Obninsk, 1972 [in Russian].

TABLE 1. EXPERIMENTAL VALUES OF AVERAGE MULTIPLICITIES AND $\alpha = \sigma_\gamma/\sigma_f$ FOR ^{235}U RESONANCES

E_0 (eV)	J	K^{av}	α[pres.]	α[2]	α[5]	E_0 (eV)	J	K^{av}	α[pres.]	α[2]	α[5]
I.460	3	3.5I	2.I3			I9.30	4	4.44	0.8I	0.68	0.76
2.028	3	3.58	3.05			I9.32	3	4.52	0.75		
3.I47	4	4.6I	0.59			20.I0	4	4.27	0.59		
3.6I0	4	4.I5	I.23	0.73		20.6I	4	4.I3	I.3I		
4.840	4	3.5I	4.64	8.26		2I.07	4	4.II	I.52	I.35	I.65
5.44	4	3.98	2.0I			22.94	4	4.36	I.I7		
6.38	4	3.7I	3.46	3.03	3.64	23.42	4	3.79	3.66		
6.95	3	3.60	2.I9			23.63	3	4.67	0.86		
7.08	4	4.I5	I.22	I.I9	I.44	24.23	3	4.I9	I.77		
8.77	4	4.72	0.56	0.40	0.44	24.50	4	4.58	0.75		
8.97	3	4.I8	0.66			24.80	4	4.66	0.55		
9.28	4	4.69	0.60	0.60	0.66	25.I9	4	4.97	0.30		
9.73	3	4.52	0.44			25.60	3	4.82	0.46		
I0.I7	4	4.39	0.66			26.49	4	4.53	0.55		
II.67	4	3.5I	6.35	7.69	8.68	26.52	3	4.84	0.55		
I2.39	3	4.I6	I.30	I.45	I.66	27.I6	3	4.3I	0.83		
I2.43	4	4.02	I.63			27.78	4	4.60	0.83		
I2.86	4	4.I6	I.07			28.00	3	4.42	0.86		
I3.25	4	4.I9	I.0I			28.36	3	4.46	0.76		
I3.70	4	4.4I	0.88			28.73	4	3.76	I.42		
I4.00	3	4.85	0.36	0.08	0.09	29.00	3	-	-		
I4.54	3	4.03	I.67			29.65	4	3.9I	I.99		
I5.40	4	4.33	0.95	0.84	0.94	30.59	3	4.I2	I.05		
I5.5I	4	3.69	2.I0			30.87	4	3.75	2.33		
I6.08	4	3.98	I.88	I.88	2.I4	3I.55	4	3.75	2.7I		
I6.70	4	4.50	0.58			32.03	4	4.47	0.80		
I8.05	3	4.50	0.72	0.35	0.33	32.07	3	4.44	I.06	0.66	0.66
I8.96	4	4.3I	0.80			33.52	4	4.I0	I.35		
33.65	3	4.I9	I.78			48.55	4	4.I4	I.35		
34.37	4	4.I8	I.I9			48.77	3	4.5I	0.9I		
34.40	3	4.48	I.0I			49.45	4	3.87	2.45		
34.86	3	4.65	0.58			50.I2	3	4.08	I.42		
35.II	4	4.63	0.22			50.40	4	4.42	0.7I		
35.20	3	4.48	0.44			50.5I	3	4.4I	0.47		
36.45	4	3.8I	I.75			5I.II	3	4.69	0.56		
37.20	3	3.82	2.I9			5I.29	4	4.67	0.68		
38.08	3	4.43	0.78			5I.63	4	4.7I	0.53		
38.36	4	4.47	0.58			52.26	3	5.05	0.I7		
39.4I	4	4.57	0.7I			52.90	4	4.55	0.86		
39.93	3	4.54	0.75			53.46	3	4.5I	0.84		
40.5I	4	4.57	0.75			54.I3	4	4.38	0.63		
4I.33	4	4.62	0.66			54.92	3	4.45	0.80		
4I.55	3	3.98	I.54			55.07	4	4.36	0.97		
4I.88	3	3.86	2.I0			55.82	4	4.87	0.36		
42.22	4	4.53	0.68			55.90	3	4.90	0.4I		
42.70	4	3.63	3.I7			56.20	3	4.77	0.52		
43.40	3	3.99	I.30			56.50	4	4.64	0.63		
43.94	4	4.48	0.76			57.66	3	4.50	0.83		
44.64	4	4.75	0.43			57.8I	4	4.68	0.62		
44.86	3	4.75	0.53			58.I0	3	4.30	I.I0		

Table 1 (continued)

E_0 (eV)	J	$K^{\pi v}$	α[pres.]	α[2]	α[5]	E_0 (eV)	J	$K^{\pi v}$	α[pres.]	α[2]	α[5]
45.82	4	4.I9	I.04			58.67	4	4.69	0.59		
46.79	4	4.36	0.80			59.73	4	4.64	0.70		
46.80	3	4.79	0.6I			60.20	3	4.77	0.42		
46.90	3	4.65	0.65			6I.I3	3	4.56	0.53		
47.02	4	4.44	0.7I			62.40	4	4.09	0.94		
47.97	4	4.29	0.95			63.56	3	4.28	0.75		
48.30	3	4.62	0.69			63.80	4	4.6I	0.56		
64.30	4	3.60	I.89			80.9	4	3.83	I.89		
65.0I	4	3.04	7.48			8I.5	3	4.50	0.67		
65.80	3	3.34	4.79			83.6	3	3.93	I.48		
66.I4	4	3.I4	9.0I			84.I	4	4.38	0.77		
66.45	4	3.58	2.8I			88.2	4	4.38	0.52		
66.52	3	3.II	I.68			88.7	3	4.43	0.73		
69.3I	4	4.58	0.6I			9I.3	3	4.37	0.79		
69.45	3	4.59	0.58			94.I	4	3.04	7.69		
70.I7	4	4.6I	0.86			97.9	4	4.I2	0.93		
70.37	3	4.77	0.47			98.I	3	4.28	0.76		
70.55	4	4.85	0.37			I02.9	4	3.38	2.90		
70.83	3	4.8I	0.68			I03.5	4	3.84	I.I5		
72.40	4	4.75	0.50			I06.I	4	4.04	I.23		
72.9I	3	4.3I	0.99			I07.6	3	3.30	4.24		
74.57	3	4.45	0.78			I09.8	4	3.26	4.98		
74.62	4	4.6I	0.67			II3.5	4	4.I5	0.68		
75.20	4	4.74	0.6I			I2I.9	4	4.25	I.00		
75.50	3	4.75	0.45			I24.8	4	4.I2	I.I8		
76.30	4	3.40	2.57			I28.2	4	4.28	I.02		
77.50	4	4.28	0.98			I3I.2	4	4.38	I.I0		
78.I0	3	4.47	0.89			I3I.6	3	4.47	0.85		
78.25	4	4.32	0.98			I35.I	4	4.45	0.69		
79.6	3	4.39	0.50			I35.4	3	4.28	0.99		
79.7	4	4.32	0.70			I4I.9	3	3.9I	I.27		
80.4	3	4.58	0.62			I45.4	3	4.04	I.I5		

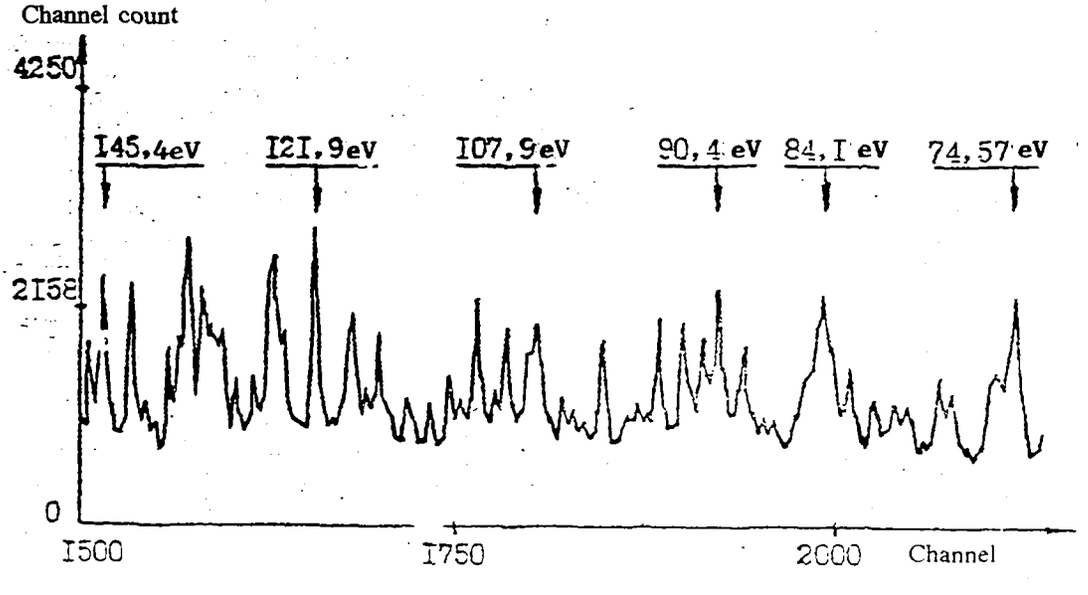

FIG. 1. Time spectrum of first gamma-ray coincidence multiplicity in the presence of background. Width of time channel 2μs.

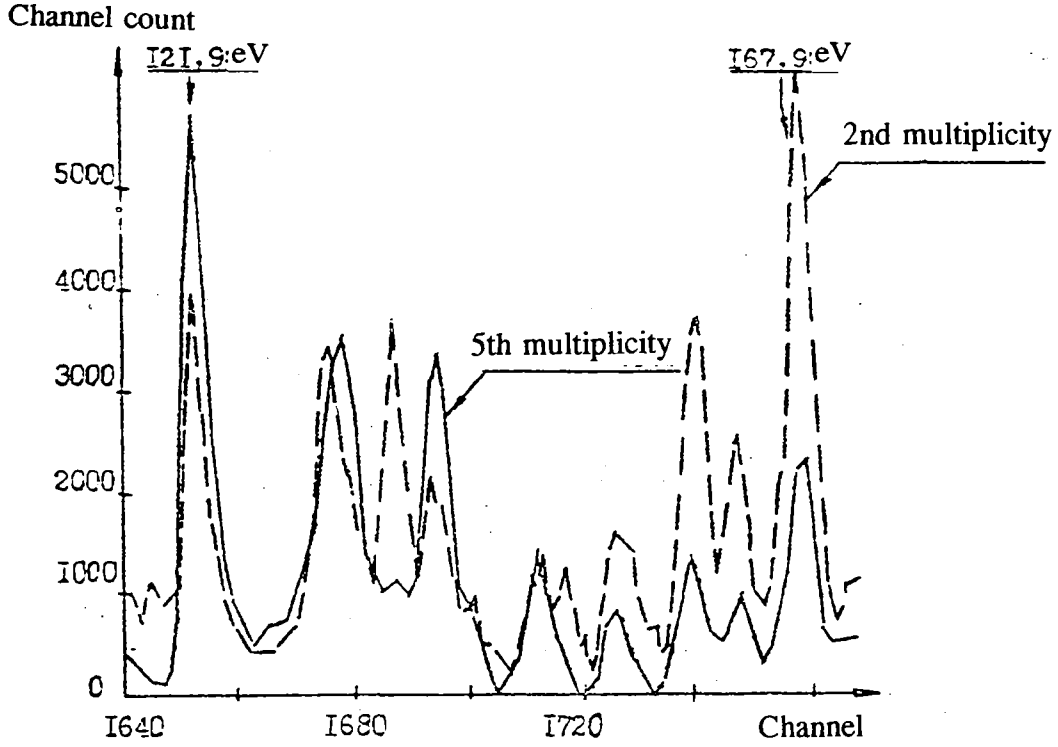

FIG.2. Time spectra of second and fifth gamma-ray coincidence multiplicity in the absence of background. Width of time channel 2 μs.

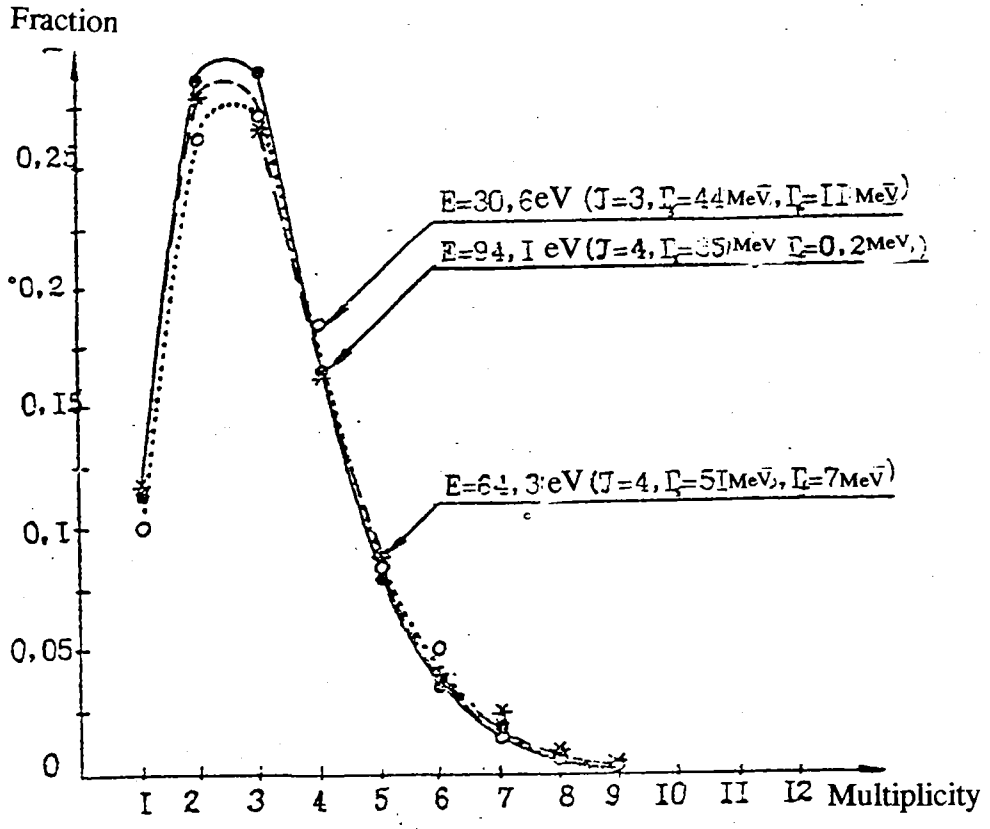

FIG. 3. Gamma-ray multiplicity spectra for resonances with small fission widths.

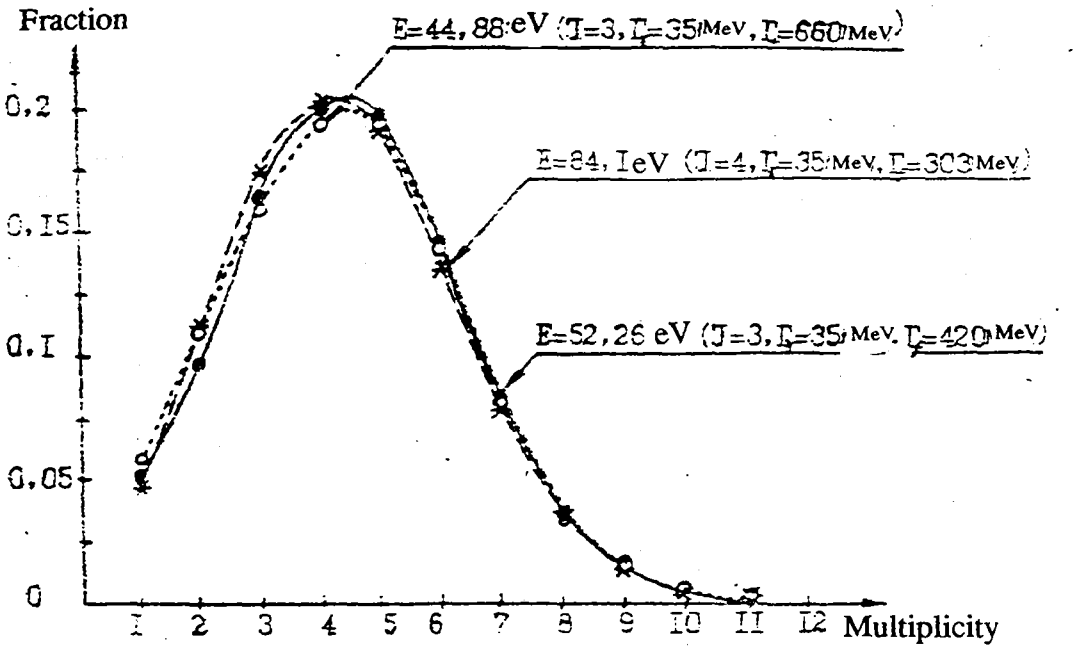

FIG. 4. Gamma-ray multiplicity spectra for resonances with large fission widths.

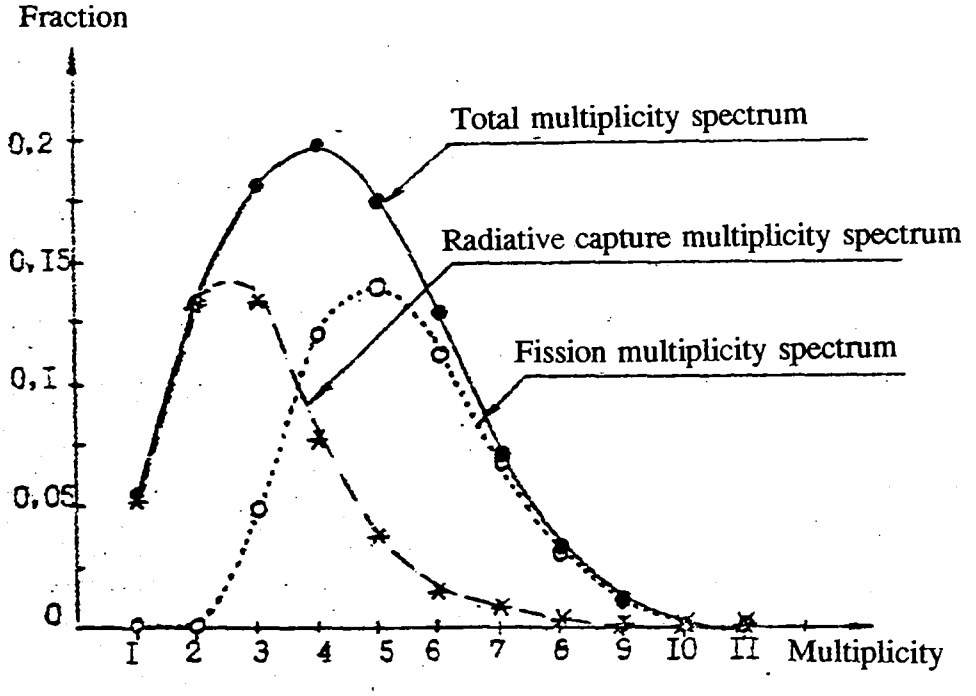

FIG. 5. Gamma-ray multiplicity spectra for a resonance with energy E = 44.6 eV (J = 4, Γ_γ = 35 MeV, Γ_f = 170 MeV).

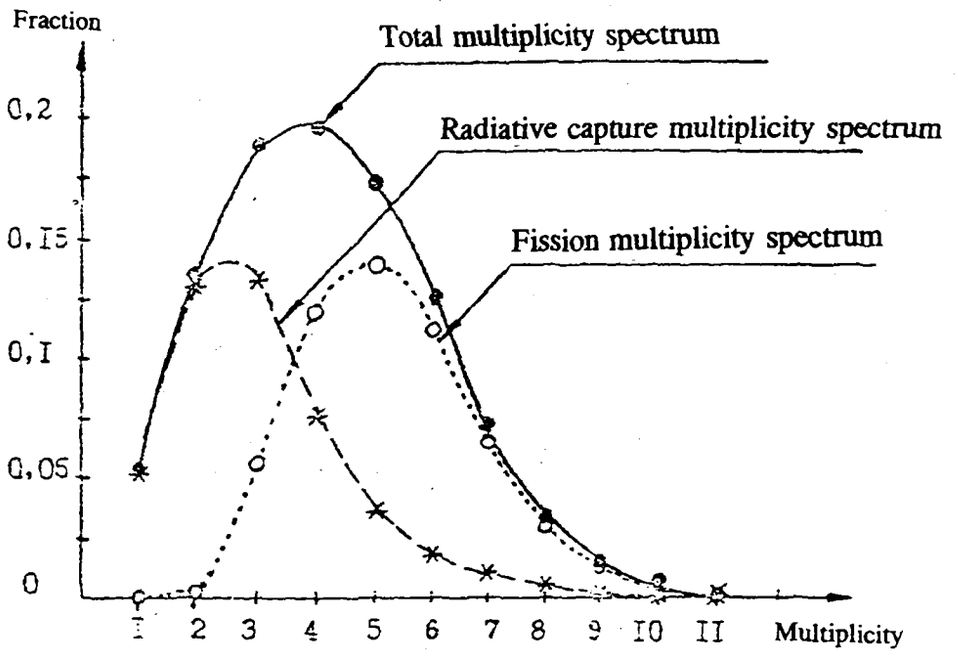

FIG. 6. Gamma-ray multiplicity spectra for a resonance with E = 72.4 eV (J = 4, Γ_γ = 35 MeV, Γ_f = 98 MeV).

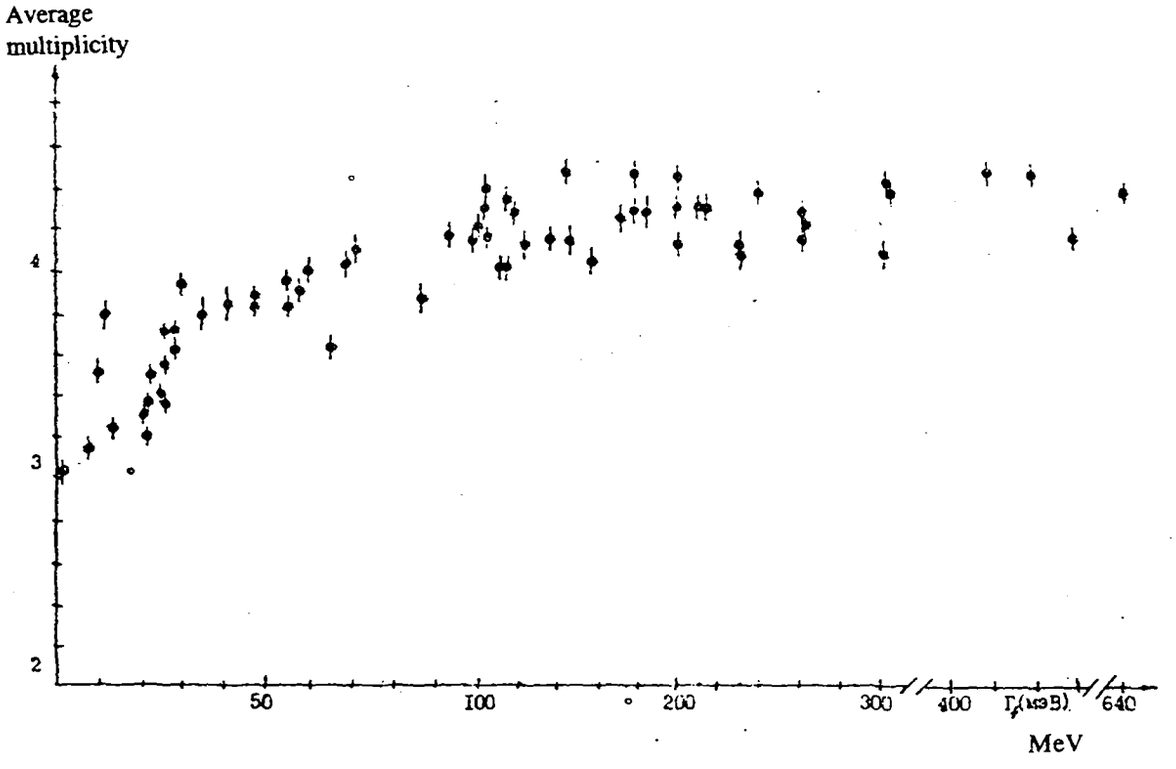

FIG. 7. Average multiplicities of total spectra as a function of fission width Γ_f

95-11660 (H+)
Translated from Russian

CROSS-SECTION OF THE REACTION $^{7}Li(p,n)^{7}Be$ CLOSE TO THE THRESHOLD

V.S. Shorin
Institute of Physics and Power Engineering, Obninsk

ABSTRACT

The status of data on the cross-section of the reaction $^{7}Li(p,n)^{7}Be$ close to the threshold is reviewed. On the basis of recent data on the cross-section of the inverse reaction $^{7}Be(n,p)^{7}Li$ and certain theoretical models, an evaluation is performed of the total cross-section of the $^{7}Li(p,n)$-reaction in the proton energy region up to 2 MeV.

The reaction $^{7}Li(p,n)^{7}Be$ ($Q = 1.644$ MeV, $E_{thr} = 1.881$ MeV) is one of the popular sources of neutrons. A study of the high-lying levels of an ^{8}Be nucleus excited in the reaction is particularly useful for developing nuclear models and multichannel versions of the theory of nuclear reactions. The reaction cross-section is also interesting for nuclear astrophysics. A great deal of information on the total cross-sections of the reaction $\sigma_{pn}(E_P)$ and the differential cross-sections $d\sigma_{pn}/d\Omega(E_p\theta)$, measured up to 1973, has been assembled and tabulated in Ref. [1]. The latter also provides an evaluation of the cross-section (accuracy ~ 5%) in the proton energy region $E_p \geq 1.95$ MeV, which has been widely used hitherto in practice. The aim of the present work is to evaluate data close to the reaction threshold ($E_p \leq 1.95$ MeV), taking new experimental and theoretical data into account.

Situation up to 1977

Early investigations of the reaction cross-section close to the threshold (relative accuracy of data ~ 1%, absolute accuracy ~ 5%) [2-5] showed that the reaction cross-section

is determined by the wide ($\Gamma \geq 500$ keV) s-resonance ($J^{\pi} = 2$, $T = 0$) close to the threshold at $E_{res} \approx 1.9$ MeV and is described well by the one-level formula ($| E_p - E_{res} | << \Gamma/2$)

$$\sigma_{pn}(E_p) = 4\pi \cdot g(J) \cdot k_p^2 \cdot x(1 + x)^{-2} \quad (1)$$

where $g(J) = 5/8$ is the spin factor and k_p is the proton wave number in the centre-of-mass system, $x = \Gamma_n / \Gamma_p = 0.106 \cdot (E_p - E_{thr})^{1/2}$, $[E_p, E_{thr}] =$ keV.

For analysing the data, we introduce the function $S(v)$:

$$S(v) = \sigma_{pn} \cdot (1 + x)^2 / v \quad (2)$$

where $v^2 = E_n^{cm} = 0.7645 \cdot (E_p - E_{thr})$ keV and E_n^{cm} is the neutron energy in the centre-of-mass system. For a cross-section, determined by the relation (1), the function $S(v)$ is equal to

$$S_1(v) = 2.5834 \cdot 10^5 \cdot E_p^{-1} \text{ [mb} \cdot \text{keV}^{-1/2}] \quad (3)$$

In Ref. [5] the function $S(v) = \sigma_{pn}/v$ was introduced. The value of $S_1(0)$ is 137.4 mb $\cdot$ keV$^{-1/2}$, and it may be easily related to the cross-section of the inverse thermal reaction ^{7}Be(n,p)^{7}Li with the aid of the principle of detailed equilibrium

$$\sigma_{pn} = \sigma_{np} \cdot 1.0014 \cdot (E_n/E_p)^{cm}. \quad (4)$$

Formula (3) describes well the experimental data of Ref. [5] in the energy region $\Delta = E_p - E_{thr} \leq 100$ keV and agrees with the cross-section $\sigma_{np} = 48000 \pm 9000$ b [6], which corresponds to the value $S(0) = 146 \pm 25$ mb $\cdot$ keV$^{-1/2}$. Some fluctuations were observed in the region $\Delta < 1$ keV only. However, the over-estimated values of the width Γ and the ratio of the reduced widths ($\gamma_n^2 / \gamma_p^2 = 5$), obtained in Refs [2, 3, 5] have raised a number of questions. Thus, in the reaction ^{7}Li(p,γ) an anomaly was observed in the cross-section close to the threshold with a width $\Gamma = 150 \pm 50$ keV [7] and the identification of the resonance $J^{\pi} = 2^-$, $T = 0$ was confirmed, whereas previous works required the

introduction of an appreciable contribution of the state with T = 1. In the scattering of ^{7}Li(p,p) an anomaly was also observed in the phase shifts of the level $^5S_2$ with a width of ~ 50 keV [8]. These anomalies were analysed in the context of the approximation of the scattering lengths for the S-matrix [8] which identified the state $J^\pi = 2^-$ as the threshold state or virtual resonance having a width of 50 ± 20 keV with the pole of the S-matrix at $k_n = -7\text{-}3 \cdot i\text{keV}^{1/2}$ in the complex plane of the neutron k_n wave numbers. The value of the cross-section σ_{np} in this approach takes the form

$$\sigma_{np} = \frac{5\pi}{8k_n^2} \cdot \frac{2k_n a_i \cdot (1 + \eta^2 b_i / a_i)}{(1 + k_n \cdot a_i)^2 + k_n^2 \cdot a_r^2}, \quad (5)$$

where a_r and a_i are the real and imaginary parts of the basic scattering length respectively; b_i is the imaginary part of the additional scattering length; and η is the module of the S-matrix element for the (p,p)-channel. The parameters a_i and $\eta^2 b_i/a_i$ are determined from the cross-section of the (n,p)-reaction at the thermal point, using the relationships

$$\sigma_{np}^{tot} = \sigma_{np} + \sigma_{np'} = \frac{5\pi}{8k_n^2} \cdot \frac{k_n \cdot a_i}{(1 + k_n \cdot a_i)^2 + k_n^2 \cdot a_r^2}, \quad (6)$$

$$\sigma_{np} = \sigma_{np'} / \sigma_{np} = (1 - \eta^2 b_i a_i) \cdot (1 + \eta^2 b_i a_i)^{-1}. \quad (7)$$

The value a_r is found from the form of the anomaly of the phase shift of the level $^5S_2$ in the scattering. On the basis of data in Ref. [6], the authors of Ref. [8] calculated the (p,n)-reaction cross-section which agrees in magnitude and form with the experimental and theoretical data of Ref. [5], i.e. reproduces the form of Eq. (1).

The same set of experimental data: (p,p), (p,p') and (p,n)-reactions was described in Ref. [9] in the context of the R-matrix theory, which is more complete than in Ref. [2]. It was shown that the state $J^\pi = 2^-$, T = 0 has a 14% contribution of the component T = 1. Thus the experimental and theoretical data close to the threshold for different channels of the interaction P+^{7}Li were consistent.

A certain problem with the experimental data arose after publication of Ref. [10] in 1966, in which the graphic data of a number of works were tabulated. In the process, errors were made in the determination of the energy scale amounting to ~ 1.35 keV [11] for the data of Refs [2-5] which proved very important in the region around the threshold. The data in Ref. [10] were automatically included in Ref. [1] and as a result the value σ_{pn} at energy $\Delta = 1$ keV became equal to 12 mb [1], whereas from Eq. (1) we obtain $\sigma_{pn} = 98$ mb, and from Fig. 6 in Ref. [5] it is evaluated as $\sim$ 94 mb. The latter value in Ref. [1] is assigned to energy $\Delta = 3$ keV. The data of Ref. [1] close to the threshold naturally contradict the established trend of the cross-section $\sigma_{pn} \infty$ x (Figs 5, 6 of Ref. [5]) and they need to be corrected. On the basis of formula (6) and the value σ_{pn}, given in Ref. [1], a correction was performed to the values of Δ in the energy region $\Delta \leq 15$ keV, the results of which are shown in Table 1.

The correction was not performed for $\Delta \geq 15$ keV, since here the error in σ_{pn}, associated with the shift, becomes less than the measuring error. The data assembled in Ref. [1] are presented in the form of values of $S(\Delta)$ in Fig. 1 together with the theoretical curve of $S_1(\Delta)$. (The data in Refs [3, 4] have been corrected). Some of the values were obtained from the tabulated values of $d\sigma_{pn}(O^0)/d\Omega$ and the coefficients of the cross-sections represented in the form of Legendre polynomials [1], using the relationships

$$\sigma_{pn}(E_p) = 4\pi \cdot A_0(E_p) \cdot [d\sigma_{pn}(E_p, 0^0)/d\Omega]^{cm}, \qquad (8)$$
$$A_0(e_p) = 1 - A_1(E_p) - A_2(E_p).$$

The values $A_1(E_p)$ and $A_2(E_p)$ were approximated by the expressions

$$A_1(\Delta) = -20\delta^2 \cdot (1 - 3.397 \cdot \Delta) \cdot (1 - 7.326 \cdot \Delta + 18.664 \cdot \Delta^2)^{-1}, \ \Delta \leq 2.1 \text{ MeV}$$

$$0, \ \delta \leq 0$$

$$A_2(\Delta) = 12.82\delta^2 \cdot (1 + 40 \cdot \delta + 25.641 \cdot \delta^2)^{-1}, \ \delta = E_p - 1.98 \geq 0 \text{ MeV}.$$

Note that the values of σ_{pn} calculated from the formulae (8) differ from the corresponding results of direct measurements (for Ref. [4]) by 1-3%. The figure clearly shows that with visible divergence of the data for different groups, the values of S(Δ) within each group are practically constant in the region $40 \leq \Delta \leq 110$ keV, amounting to ≈ 130 mb · keV$^{-1/2}$. The biggest difference is shown by the data in Ref. [12], for which $S \approx 115$ mb · keV$^{-1/2}$. The remaining data lie in the 5% error corridor. In the energy region $\Delta < 30$ keV the data of Ref. [2] deviate appreciably from the theoretical curve of $S_1(\Delta)$, which indicates the need to revise the original data and correct the tabulated values of Δ in Ref. [1] pertaining to Ref. [2]. For the rest, the conclusions drawn earlier on the agreement between theoretical and experimental data (up to 1977) are confirmed.

Situation after 1988

In 1988 new and more accurate data appeared for the cross-section of the (n,p)-reaction in the energy region 25 meV ≤ E ≤ 13.5 keV [11], which gave the value of the cross-section at the thermal point as $\sigma_{np} = 38\,400 \pm 800$ b and the corresponding value $S(0) = 116.9 \pm 2.4$ mb · keV$^{-1/2}$. The reaction cross-section is described well by the formula:

$$\sigma_{np}(E_n) = (5/8)\cdot(4\pi/k_n^2)\cdot y\,(1+y)^{-2}, \qquad (9)$$

where $y = (3.96 \pm 0.15)\, E_n/(E_p)^{1/2}$; Eq. (9) enables the expression for the function S(v) in the energy region $E_n \leq 13.5$ keV to be written:

$$S_2(v) = 9653\cdot(1+x)^2\cdot(1+y)^{-2}\cdot E_p^{-3/2}\ 6\cdot \text{keV}^{-1/2}. \qquad (10)$$

The functions $S_2(v)$ and $S_1(v)$ have an appreciably different energy trend and differ from each other by 7-17% (see figure). Such divergences go beyond the error limits and make it necessary for new experiments to be carried out.

The authors of Ref. [11] carried out an R-matrix analysis of the data obtained and data on cross-sections and polarization for the reactions ^{7}Li(p,n) and ^{7}Li(p,p) in the energy region $E_p < 3$ MeV, using a charge-symmetric multichannel multilevel formalism. This analysis made it possible not only to describe well the whole set of data but also to determine the parameters of the threshold state, which is closely merged with the high lying state $J^\pi = 2^-$, $T = 1$ at $E_p \approx 5.4$ MeV. The threshold state was "virtual" (the pole of the S-matrix lies in a non-physical plane in which the complex value of k_p has a positive imaginary part and k_n a negative one). The resonance energy lies 10 keV below the threshold. The virtuality of the resonance leads to an unusual relationship between its widths: $\Gamma_p = 1408$ keV, $\Gamma_n = 223$ keV, $\Gamma = 122$ eV $<<$ $\Gamma_n + \Gamma_p$. The total width appears only in cross-sections for open channels (p,p), (p,α) and (p,γ). For the closed (p,n)-channel the cross-section is determined by the large value of Γ_p in agreement with the conclusions of Ref. [2]. Thus, application of a more complete model has made it possible to remove practically all the apparent contradictions between the theoretical and experimental data.

In Ref. [11] the theoretical R-matrix cross-section of the (n,p)-reaction is given only in the region $E_n < 13.5$ keV. It is to be noted that it goes 2% below the experimental data in the region $E_n < 2$ keV and 2% above the cross-section given by formula (9) at energy 13.5 keV. This poses the problem of extrapolating the R-matrix curve into the energy region $\Delta = 13.5$-100 keV. The simplest means of extrapolating is to use formula (10). In this case the calculated S_2-values converge with the S_1-values with increase in Δ, and the difference between them amounts to $\leq 2\%$ at $\Delta > 50$ keV, as can be seen from the figure. The other method of extrapolating takes into account the difference between the R-matrix curve and the curve of S_2 in the region $E_n < 13.5$ keV and its asymptotics,

i.e. approximation to experimental data in the high-energy region. Using relation (3) and the connecting function f(ν), we obtain the desired function $S_3(\nu)$:

$$S_3(\nu) = S_1(\nu) \cdot f(\nu), \tag{11}$$

where $f(\nu) = 0.8467 + 0.15338 \cdot \nu^2 \cdot (\nu^2 + 5.209)^{-1}$. Evidently $f(\nu) \to 1$ with $\nu \to \infty$. Even at $\Delta = 30$ keV the calculated S_3-function differs from the S_1-curve by 2.7%, the difference reducing to 1% at $\Delta = 100$ keV. The difference between curves S_2 and S_3 does not exceed 2%.

The concept of the threshold state in Ref. [8] provides another method of approximation. Using the new data in Ref. [11] for the values σ_{np}^{tot} and α_{np} and the relations (6) and (7), we find:

$$\eta^2 \cdot b_i/a_i = \begin{array}{l} 0.977 \pm 0.001 \text{ - from averaged data} \\ 0.980 \pm 0.006 \text{ - from the thermal point} \end{array}$$

$a_i \cdot k_n^{th} = 4.62 \cdot 10^{-4}$, $a_i = 0.106 \pm 0.002$ keV$^{-1/2}$

Earlier these parameters were given in Ref. [8] as: $\eta^2 \cdot b_i/a_i = 0.96 \pm 0.02$, $a_i = 0.12 \pm 0.02$ keV$^{-1/2}$. Here and below for the values a and k_n a system of units from Ref. [8] is used in which $k_n \equiv v \equiv (E_n^{cm})^{1/2}$. Using the value of $a_r = 0.04$ keV$^{-1/2}$ [8], we find the pole of the S-matrix at the point $k = -8.3 - i \cdot 3.1$ keV$^{1/2}$, which corresponds to the Breit-Wigner width $\Gamma = 104$ keV (earlier 84 keV [8]). The cross-section of the (n,p)-reaction as per Eq. (5) takes the form:

$$\sigma_{np} = 194{,}6 \cdot E_n^{-1/2} \cdot [(1 + 0{,}09248 \cdot E_n^{1/2}) + 0{,}0012 \cdot E_n]^{-1} 6, \tag{12}$$

where $[E_n]$ = keV. The cross-section calculated from formula (12) is 1% lower than the value calculated from formula (9) for $E_n = 10$ keV. At $E_n < 1$ keV the difference between them is less than 0.2%. Using Eq. (12) to evaluate the cross-section of the (p,n)-reaction, we find:

$$S_4(v) = \frac{223 \cdot (1 + 0{,}12123 \cdot v)^2}{E_p^L \cdot [(1 + 0{,}1058 \cdot v)^2 + 0{,}0016 \cdot v^2]} \text{ б} \cdot \text{keV}^{-1/2}, \qquad (13)$$

where $[E_p^L] = \text{keV}$. The function S_4 (see figure) goes 4% lower than the curve of S_1 at $\Delta = 100$ keV and 8% lower at $\Delta = 15$ keV. The divergence with the curve of S_3 amounts to $\approx 3.5\%$ at $\Delta > 15$ keV. Since in the concept of the threshold state the contribution of distant resonances is not taken into account, the function $S_4(\Delta)$ may be considered the minimum evaluated value of the (p,n)-reaction cross-section in the energy region $\Delta > 13.5$ keV. Since the R-matrix curve [11] goes higher than the experimental data at $\Delta > 10$ keV, the function $S_4(\Delta)$ is more truly the maximum evaluated value for the cross-section σ_{pn}.

In conclusion, it is to be noted that, when the 5% accuracy of absolutization of the (p,n)-data of the basic works [2-5] is taken into account, the contradictions between experimental data for the direct reaction and the evaluated data for the inverse reaction in the energy region $\Delta > 25$ keV practically disappears. At the same time, in the energy region $\Delta < 13$ keV clear discrepancies exist (if the principle of detailed equilibrium is not called into question) among existing experimental data, so that new measurements of the total cross-section of the ^{7}Li(p,n)-reaction close to the threshold are definitely required.

REFERENCES

1. Liskien H., Paulsen A./At.Data and Nucl.Data Tables, 1975, v.15, p.57-84.
2. Newson H.W., Williamson R.M., Jones K.W. e.a./Phys.Rev., 1957, v.108, p.1294.
3. Macklin R.L., Gibbons J.H./Phys.Rev., 1958, v.109, p.105-109.
4. Gibbons J.H., Macklin R.L./Phys.Rev.,1958, v.114, p.571.
5. Gibbons J.H., Newson H.W. In: Fast Neutron Physics. N.Y., Interscience, 1960, v.1, p.133.
6. Hanna R.C./Philos.Mag., 1955, v.45, p.381.
7. Sweeney W.E.,Jr., Marion J.B./Phys.Rev., 1969, v.182, p.1007.
8. Arnold L.G., Seyler K.G., Brown L., e.a./Phys.Rev. Letters, 1974, v.32, p.895-898.
9. Barker F.C./Austr.J.Phys.,1977, v.30, p.113.
10. Kim H.J., Milner W.T., McGowan F.K./Nucl.Data Tables, 1966, v.A1, p.203.
11. Koehler P.E., C.D.Bowman, Steinkruger F.J. e.a./Phys.Rev.,1988, v.C37, no.3, p.917-926.
12. Levefre H.W., Din G.U./-Austr.J.Phys., 1969, v.22, p.649.
13. Austin S.M./Bull.Am.Phys.Soc.,1962, v.7, p.269.
14. Gabbard F., Davis R.M., Bonner T.W./Phys.Rev., 1959, v.114, p.201.
15. Peetermans A. Thesis. University Liege, 1970.
16. Hunt J.B., Robertson J.C. In: Proc.of the first symp. on neutron dozimetry in biology and medicine. Neuherberg, 1972, p.935.

Table 1

Values							
Before correction				After correction			
Δ, keV	σ_{pn}, mb	ν, keV$^{1/2}$	$S(\nu)$, mb· keV$^{1/2}$	Δ, keV	ν, keV$^{1/2}$	$S(\nu)$, mb· keV$^{1/2}$	$S_1(\nu)$, mb· keV$^{1/2}$
1.0	12.0	0.874	16.8	0.01	0.087	140.7	137.3
3.0	94.0	1.514	87.0	0.9	0.829	137.3	137.3
4.0	146.0	1.749	122.7	2.9	1.489	136.7	137.2
5.0	171.0	1.955	133.9	4.6	1.875	137.4	137.1
6.0	190.0	2.142	140.7	6.6	2.246	136.9	136.9
9.0	207.0	2.623	137.1	9.1	2.637	136.7	136.7
11.0	221.0	2.900	139.2	12.0	3.029	136.4	136.5
15.0	237.0	3.386	139.3	16.8	3.584	136.1	136.1

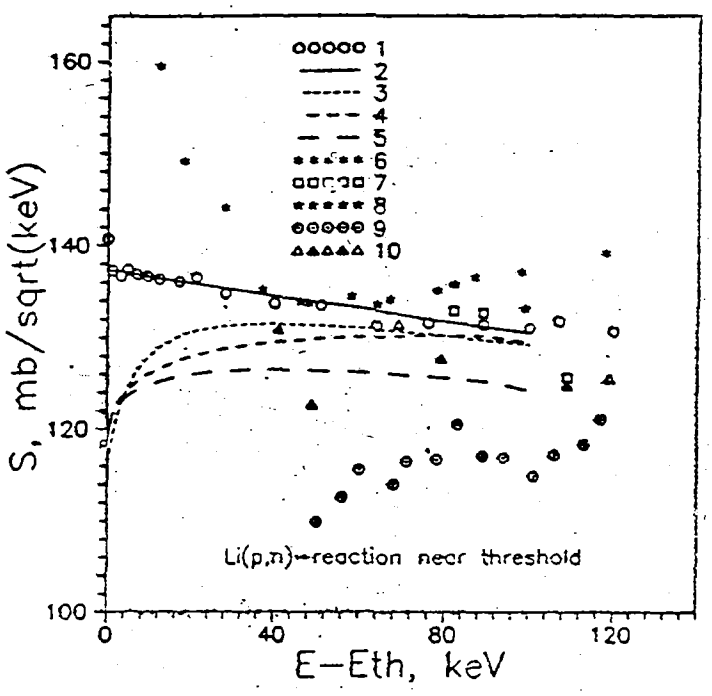

FIG.1. Experimental and theoretical values of S(v) versus the value by which proton energy exceeds the threshold of the $^7Li(p,n)$-reaction. The theoretical curves 2 = S_1, 3 = S_2, 4 = S_3 and 5 = S_4 were calculated from formulae (3), (11), (10) and (13) respectively. The experimental data were derived as follows: 1 from Refs [3, 4], 6 from Ref. [2], 7 from Ref. [13], 8 from Ref. [14], 9 from Ref. [12] and 10 from Ref. [15] (light symbols) and from Ref. [16] (dark symbols).

95-11660 (H+)
Translated from Russian

UDC 539.173.12

FISSION CROSS-SECTIONS OF ^{235,238}U AND ^{209}Bi AT INCIDENT PROTON ENERGIES ABOVE 70 MeV

A.I. Obukhov, A.A. Rimskij-Korsakov and V.P. Eismont
V.G. Khlopin Radium Institute
St. Petersburg

ABSTRACT

The proton fission cross-section data of ^{235,238}U and Bi were measured in the V.G. Khlopin Radium Institute over a wide proton energy range. The experimental and calculated data were also compared with experimental neutron values. The proton cross-section of ^{235,238}U increased up to 60-70 MeV and then decreased. The bismuth proton fission cross-section increased in line with the rise in proton energy up to 1 GeV.

Information on the dependence of the fission cross-sections of nuclei on incident proton energy in the intermediate energy region is important both for an understanding of the mechanism of competition between fission and spallation as well as for applied tasks such as, in particular, the production of intense neutron sources for transmutation of radioactive waste. The data available in the literature on the energy dependence of the fission cross-sections of nuclei irradiated with protons with an energy of over 100 MeV are very contradictory.

The results of Steiner and Jungerman (1956) [1] showed that the 100-340 MeV proton induced fission cross-sections of the ^{238}U and ^{235}U nuclei remained constant at around 1.4 b. Later, in 1961, Perfilov presumed that the fission cross-sections of these nuclei or, more precisely, their fissionability, σ_f/σ_{in}, remained approximately constant even when the incident proton energy rose above 340 MeV [2]. Later measurements of the fission cross-sections of

^{238}U performed by several groups of researchers in 1965-1976 yielded several variants of the energy dependence of the fission cross-sections ranging from the variant where it remained constant right up to 10 GeV [3] to several variants where it changed and where the fission cross-sections of these nuclei decreased with increase in proton energy [4-7] (Fig. 1). Apart from Ivanova's measurements [4], who used nuclear emulsions, in the remaining cases (Fig. 1) the fission fragments were recorded using sandwich-type detectors comprising two solid state detectors, mica [3], macrofol [7] and silicate glass [5]. One of the possible causes of the divergence of the measurement results shown in Fig. 1 is uncertainty regarding the identification of the tracks of fission fragments flying in the direction of the detector plane and slowed down in the detector. The comparison of the results from two different methods of counting fission fragment tracks in the same detector performed by Hudis and Katcoff in 1969 and 1976, respectively, makes this clear [6] (Fig. 1). There was a large spread of values in the energy dependence of the fission cross-sections of bismuth nuclei irradiated with protons with energies above 70 MeV. At the Radium Institute several series of fission cross-section measurements were carried out for uranium, thorium, bismuth, lead, gold and tantalum nuclei irradiated with 70, 100, 155, 200 MeV and 1 GeV protons [8, 9]. The irradiation with 70-200 MeV protons was performed using an extracted beam from the synchrotron at the Institute of Theoretical and Experimental Physics, and the irradiation with 1 GeV protons was performed using an extracted beam from the phasotron at the Leningrad Nuclear Physics Institute. The circular geometry of positioning the silicate glass detectors ensured 100% recording of the fission fragments from the nuclei under investigation. The 70-200 MeV proton beam was monitored using a calibrated induction sensor with an accuracy of 5%; the 1 GeV proton beam was monitored using a Faraday cylinder with an accuracy of 3%.

Recently, the 10-100 MeV proton induced fission cross-sections of heavy nuclei from thorium to americium were measured by another group using the proton synchrotron at the Radium Institute [10]. Figure 2 shows the experimental data on the 9 GeV proton induced fission cross-sections of ^{238}U nuclei obtained earlier using the nuclear emulsions method [11]. As can be seen from the figure, the fission cross-section for ^{238}U nuclei has a maximum in the 50-70 MeV energy range followed by a decline up to a proton energy of 9 GeV. Figure 2 also shows the 200 MeV neutron induced fission cross-section values for ^{238}U nuclei which were obtained experimentally by Lisowski et al. [12]. Just as in the case of protons, the fission cross-section has a maximum only at a lower neutron energy - around 30-40 MeV - and its value at the maximum is lower. It also gives the calculated value of the fission cross-section of ^{238}U nuclei as a function of neutron energy over a wide range up to 9 GeV [13]. A qualitative similarity can be seen in the dependence of the fission cross-sections in the three cases, but there is a shift in the value and shape of the dependence. Figure 3 shows similar dependences of the proton- and neutron-induced fission cross-sections of ^{235}U nuclei [8, 9, 12-14].

Eismont et al. [14] found that the fissionability σ_f/σ_{in} of ^{238}U and ^{235}U nuclei increased with proton energy from the Coulomb barrier, reaching saturation at proton energies of 30-50 MeV. The dependence of the cross-section for inelastic interaction of protons with uranium nuclei σ_{in} was taken from the systematics of Barashenkov [15]. According to these systematics, the cross-sections for inelastic interaction of protons with uranium nuclei pass through a maximum near a proton energy of 40 MeV and then slightly decrease, going through a minimum in the 200-300 MeV region, and then it increases again insignificantly. Figure 4 shows the dependence of the fissionability of ^{238}U nuclei on proton energy. A similar dependence of σ_f/σ_{in} is observed in the case of ^{235}U nuclei. Thus, the fissionability

of uranium nuclei rises from the Coulomb barrier, reaches saturation, and then at incident proton energies above 100 MeV begins to decrease as a result of the decrease in the fission cross-section of the nuclei (Figs 2, 3).

In Fig. 5 we compare the obtained experimental dependence of the fission cross-sections of ^{238}U nuclei on proton energy with a number of calculated dependences [16-19]. There is a fairly good qualitative agreement between the experimental and calculated dependences.

Figure 6 shows the experimentally obtained dependence of the fission cross-sections of bismuth nuclei on proton energy up to 1 GeV [8, 9]. The evaluated dependence $\sigma_f(E_p)$ is also shown [20]. Up to 200 MeV, the experimental data obtained at the Radium Institute agree satisfactorily with the evaluated dependence, however they diverge noticeably at higher energies.

Figure 6 also shows the cross-section values for fission of bismuth nuclei induced by 135 and 160 MeV neutrons [21]; these are evaluated as preliminary data. The cross-sections for fission of bismuth nuclei induced by neutrons are lower approximately by a factor of three than those by protons of corresponding energies. However, the ratio of the evaluated values $\sigma_f(E_p)/\sigma_f(E_n)$ is two [20].

Thus, on the basis of the experimental data obtained at the Radium Institute on the proton-induced fission cross-sections of ^{238}U and ^{235}U nuclei over a wide-range of energies, it has been established that the fission cross-sections of these nuclei increase with proton energy, pass through a maximum at a proton energy of 50-70 MeV, and then noticeably decrease. In the case of much lighter nuclei such as those of bismuth, the fission cross-sections continue to increase up to a proton energy of 1 GeV. Since the cross-section of inelastic interaction of protons in the 70-1000 MeV energy range with lead-type nuclei

changes very little [15], the increase from 50 to 180 mb in the fission cross-sections for bismuth nuclei over this range indicates a corresponding increase in the fissionability σ_f/σ_{in} of these nuclei.

REFERENCES

[1] STEINER, H.M., JUNGERMAN, J.A., Phys. Rev., **101** (1956) 810.

[2] PERFILOV, N.A., Zh. Ehksp. Teor. Fiz. **41** (1961) 871.

[3] BTANDT, R., et al., Phys. Rev. Appr. **17** (1972) 243.

[4] IVANOVA, N.S., Zh. Ehksp. Teor. Fiz. **31** (1956) 413.

[5] KON'SHIN, V.A., et al., Yad. Fiz. **2** (1965) 682; **7** (1968) 1187.

[6] HUDIS, J., KATCOFF, S., Phys. Rev., **180** (1969) 1122, ibid. **13** (1976) 1961.

[7] REMY, G., et al., Nucl. Phys., **A163** (1971) 583.

[8] SHIGAEV, O.E., et al., Preprint, Radium Institute, R1-17 (1973) (in Russian).

[9] BOCHAGOV, B.A., et al., Yad. Fiz. **28** (1978) 572.

[10] SMIRNOV, A.M., et al., Proc. of the 21st symposium on Nucl. Phys., Gaussing, Germany, 4-8 November 1991, 214.

[11] PERFILOV, N.A., et al., Zh. Ehksp. Teor. Fiz. **38** (1960) 716.

[12] LISOWSKI, P.W., et al., Proc. of the Specialists' meeting on neutron ccross-section standards for the energy region above 20 MeV, Uppsala, Sweden, 21-23 May 1991, 177.

[13] PRAEL, R.E., Ref. 15 in [12].

[14] EJSMONT, V.P., et al., "Cross-sections for fission of heavy nuclei induced by intermediate-energy protons, and fissionability of excited nuclei", paper presented at the Int. Conf. on Nuclear Data for Science and Technology, Gatlinburg, USA, 9-13 May 1994 (in Russian).

[15] BARASHENKOV, V.S., JINR Communication P2-89-770 (in Russian).

[16] ARTHUR, E.D., YOUNG, P.G., Calculated medium energy fission cross-sections. In: Proc. of the Conf. on Fifty Years with Nuclear Fission, Gaisersburg, M.D., ed. by J. Behrens, A.D. Carlson (1989) 931.

[17] ALSMILLER, R.G., et al., Nucl. Sci. Eng., **79** (1981) 147.

[18] ARMSTRONG, T.F., FILGES, A., In: Proc. of the 5th meeting of the Intern. collaboration on advanced neutron sources, ICANS-V, (1981), Julich, ed. by G.S. Bauer, D. Gilges, 281.

[19] BARASCHENKOV, V.S., et al., Nucl. Phys., **222** (1974) 204.

[20] FUKAHORI, T., PEARLSTEIN, S., Evaluation at the medium energy region for ^{208}Pb and ^{209}Bi. In: Proc. of the advisory group meeting organized by the IAEA, Vienna 9-12 October 1990. Intermediate energy nuclear data for application, ed. by N.P. Kocherov, INDC(NDS)-245, IAEA (1991) 93.

[21] CONDO, H., ELMGREN, K., NILSSON, J., OLSSON, N., et al., Neutron-induced fission cross-sections of ^{209}Bi and the intermediate energy region, Report at the Conference on Nucl. Data for Science and Technology, Gatlinburg, USA, 9-13 May 1994.

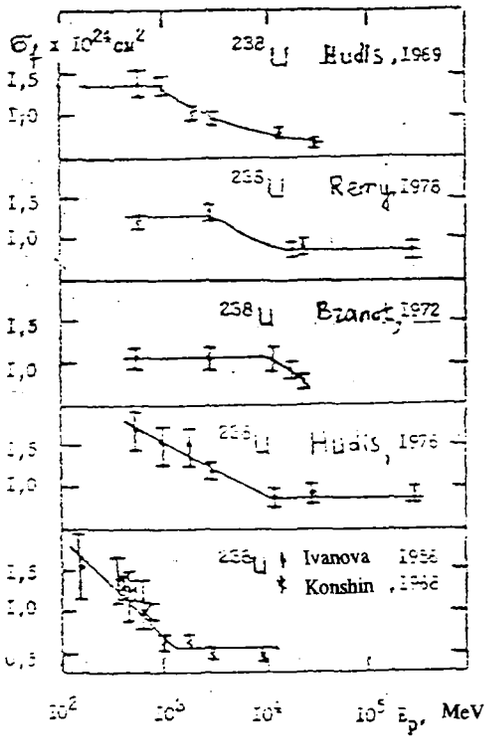

FIG. 1. Dependence of the fission cross-section of ^{238}U nuclei on proton energy from Refs [3-7].

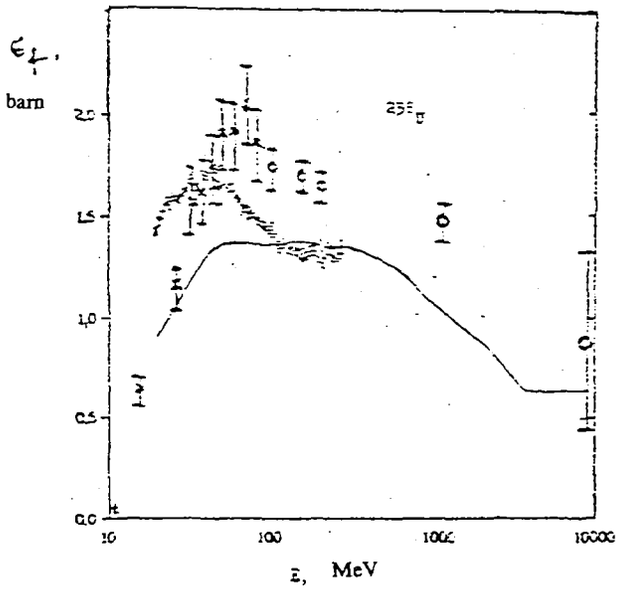

FIG. 2. Comparison of the proton- and neutron-induced fission cross-sections of ^{238}U nuclei. x - experimental values of $\sigma_f(p)$ [10]; o - experimental values of $\sigma_f(p)$ [8, 9, 11]; • - experimental values of $\sigma_f(n)$ [12]; continuous curve - calculated dependence $\sigma_f(n)$ [13].

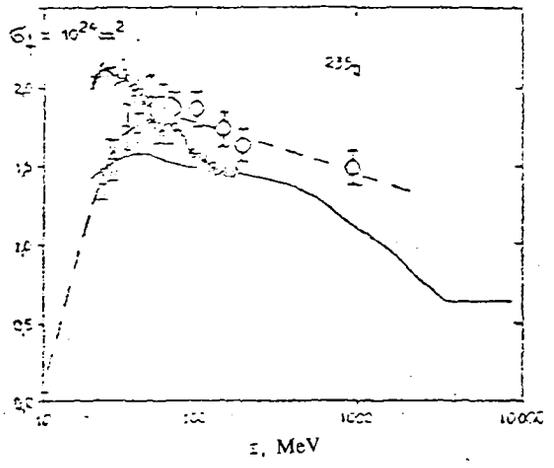

FIG. 3. Comparison of the proton- and neutron-induced fission cross-sections of ^{235}U nuclei. I - experimental values of $\sigma_f(E_p)$ [14]; o - experimental values of $\sigma_f(E_p)$ [8, 9]; x - experimental values of $\sigma_f(E_n)$ [12]; dashed line - experimental dependence $\sigma_f(E_p)$; continuous line - calculated dependence $\sigma_f(E_n)$ [13].

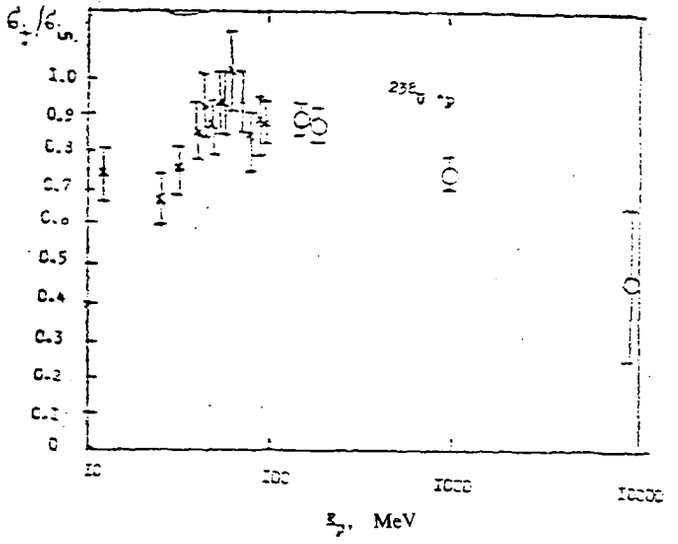

FIG. 4. Dependence of the fissionability of ^{238}U nuclei on proton energy. I - results from Ref. [10]; o - results from Refs [8, 9, 11].

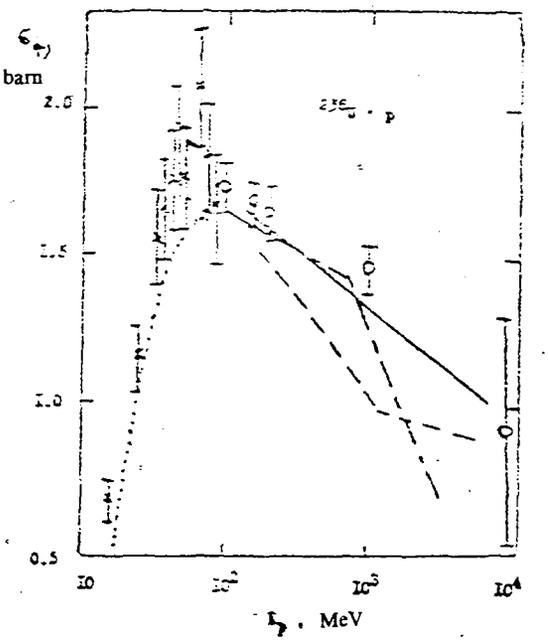

FIG. 5. Comparison of the experimental values of the proton-induced fission cross-sections of ^{238}U nuclei with the calculated values. I - experiment, $\sigma_f(p)$ [10]; o - experiment, $\sigma_f(p)$, [8, 9, 11]. Calculated dependences: continuous line - Ref. [19], dotted line - Ref. [16], dashed line - Ref. [18], dot-dash line - Ref. [17].

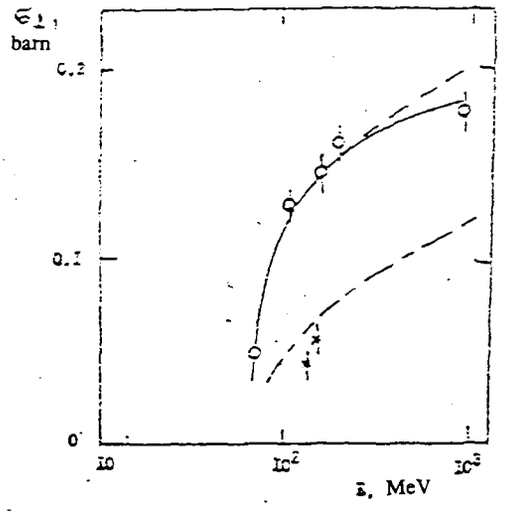

FIG. 6. Comparison of the proton- and neutron-induced fission cross-sections of ^{209}Bi nuclei. o - experiment, $\sigma_f(p)$ [8, 9]; x - experiment, $\sigma_f(n)$ [21]. Evaluated dependences: dashed line - $\sigma_f(p)$, [20], dot-dash line - $\sigma_f(n)$ [20].

Nuclear Data Section
International Atomic Energy Agency
P.O. Box 100
A-1400 Vienna
Austria

e-mail, INTERNET: SERVICES@IAEAND.IAEA.OR.AT
fax: (43-1)20607
cable: INATOM VIENNA a
telex: 1-12645 atom a
telephone: (43-1)2060-21710

online: TELNET or FTP: IAEAND.IAEA.OR.AT
username: IAEANDS for interactive Nuclear Data Information System
username: ANONYMOUS for FTP file transfer
username: FENDL for FTP file transfer of FENDL files
For users with web-browsers: http://www-nds.iaea.or.at